Journal of Computational Physics **158,** 186–213 (2000)
doi:10.1006/jcph.1999.6414, available online at http://www.idealibrary.com on IDEAL®

A Semi-implicit Semi-Lagrangian Scheme Using the Height Coordinate for a Nonhydrostatic and Fully Elastic Model of Atmospheric Flows[1]

Luca Bonaventura

Dipartimento di Ingegneria Civile ed Ambientale, Laboratorio di Matematica Applicata, Università degli Studi di Trento, Mesiano di Povo 38050 (TN), Italy, and CIRM-ITC, Povo, 38050 (TN), Italy
E-mail: bonavent@ing.unitn.it

Received April 20, 1999; revised November 10, 1999

A semi-implicit, semi-lagrangian algorithm suitable for the simulation of the dry, adiabatic, nonhydrostatic atmospheric dynamics is introduced and analysed. Height is used as vertical coordinate, without the customary terrain following normalization, thus resulting in a stable, robust, and efficient numerical scheme which allows for applications to mesoscale flows over complex orography. Results of simulations in typical lee waves test cases are presented, which show good agreement with the corresponding analytical solutions. © 2000 Academic Press

Key Words: semi-implicit; semi-Lagrangian; mesoscale models; stratified flows over complex orography; height coordinate.

1. INTRODUCTION

The high resolution simulation of atmospheric flows over complex orography poses many difficult numerical problems. Mesoscale and cloud scale simulations require the use of nonhydrostatic equations, so that sound waves must be either filtered by the anelastic approximation or dealt with numerically, for example, by semi-implicit or split-explicit methods (see, e.g., [9, 16]). Both these approaches have their respective shortcomings, those of semi-implicit methods being mainly connected to the complex structure of the three-dimensional Helmholtz equations to be solved at each timestep; see, e.g., the discussion in [35]. The choice of model equations which effectively select a particular spatial scale should then be avoided, if the aim of a consistent use of the same model from the synoptic scale down to smaller scales is to be pursued (see [42] and the models presented in [37]). An accurate

[1] This research has been partly carried out at the *GKSS Forschungszentrum*, Institut für Gewässerphysik, 21502 Geesthacht (D), within the *Training and Mobility of Researchers Program*, of the European Commission, Contract ERBFMBICT 961555.

0021-9991/00 $35.00

description of the lower boundary is obviously necessary, but the use of customary terrain following vertical coordinate systems may induce large truncation errors (see, e.g., [41]) and create conditioning problems for semi-implicit methods around very steep orography. A further requirement is that of a straightforward and efficient implementation on massively parallel computers, one of the main computational tools available both for operational and research purposes.

In this paper, a numerical scheme for the equations of a dry, adiabatic, nonhydrostatic atmosphere is presented, which aims at providing a possible solution to some of these problems by an appropriate choice of the vertical coordinate and of the lower boundary discretization. The nonhydrostatic equations are considered in advection form and the height above mean sea level, z, is used as the vertical coordinate, without employing the customary terrain following normalization. The lower boundary is discretized by an approach which has been quite successful in estuarine modelling (see, e.g., [5–7]) and which yields an accurate representation of the lower boundary without any complication of the dynamical equations because of metric terms. All the computational cells in the present discretization are rectangular boxes. The thickness of the bottom cells is allowed to vary and may assume any nonnegative value. The orographic heights are assigned at the cell sides, and the possibly different values at each side of the cell are taken into account in a finite volume discretization of the pressure equation. Exact boundary conditions can then be imposed on the prognostic variables in a simple way. In the context of the analysis of boundary discretizations of [1], the present approach is somewhere in between the *partial step* approach and the *piecewise slope representation*. The computational cells are not intersected by the slopes, as it would happen in models with a full finite volume discretization. On the other hand, although the orographic profile is approximated by a step mountain, piecewise linear slopes are implictly taken into account in the finite volume discretization of the pressure equation. It is also to be remarked that the present treatment of the lower boundary has nothing in common with the *step-mountain coordinate* proposed by Mesinger (see, e.g., [22]), which employs a pressure based vertical coordinate.

A two timestep, semi-implicit, semi-lagrangian time discretization is then introduced. For the implicit part, a weakly nonlinear algebraic system is obtained, which is symmetric and well conditioned. A fixed point iteration procedure is proven to converge to the discrete solution at each timestep under suitable assumptions. Simple and efficient solvers can be applied for the iterative solution, such as the preconditioned conjugate gradient method, thus reducing one of the heaviest computational tasks. The von Neumann stability analysis yields unconditional stability for the proposed method.

Since the proposed scheme is expected to be especially appropriate for simulation of mesoscale flows, various numerical tests have been carried out in the case of two-dimensional stratified flows over idealized mountains and development of thermals. The results obtained are in good agreement with the corresponding analytical solutions or asymptotic expansions, provided that the lower boundary is sufficiently well approximated by the computational grid, which is shown to happen at grid spacings that are realistic for high resolution models. Furthermore, one or two nonlinear iterations are usually sufficient to reach convergence at each timestep, thus showing that there is no loss in efficiency due to the solution of the nonlinear system.

The semi-implicit time discretization of the Euler equations has been used in atmospheric modelling in [9, 43]. The application of semi-lagrangian techniques to mesoscale simulations has been questioned (see, e.g., [2]), but various such models exist and others are

currently being developed (see, e.g., [10, 28, 32, 33, 42]). As remarked in [11], in spite of the problems at horizontal Courant numbers larger than one when dealing with stationary solutions, timesteps three to six times larger than those of typical Eulerian schemes are still allowed by the semi-lagrangian approach. Furthermore, the use of cells with arbitrary thickness for the vertical discretization implies that high vertical Courant numbers can easily arise, so that the semi-lagrangian approach is a quite convenient choice for a fully multidimensional discretization of the advection terms. It is however to be remarked that the semi-implicit discretization proposed in this paper is independent of the choice of the advection scheme, so that, for example, the good properties of the algebraic system obtained still hold if an Eulerian scheme is used for advection. A numerical scheme using the proposed lower boundary discretization coupled to a split-explicit time discretization and Eulerian advection is currently been investigated by J. Steppeler of the Deutscher Wetterdienst and a similar approach has also been used in a mesoscale model developed by G. Tripoli at University of Wisconsin (see [38, 45]).

The greatest inconvenience of the non-normalized vertical coordinate z is well known to be the practical difficulty to obtain a uniform resolution close to the Earth's surface. Due to the limitations of previously available hardware, this leads to an almost universal use of terrain following coordinates both for synoptic and mesoscale models. However, the use of properly stretched vertical discretization grids allows us to reach uniform resolution below a given reference height and to enlarge progressively the discretization step above. If the main contribution to the global boundary fluxes is due to terrain below some reference height, as it can be assumed, for example, in a mesoscale model when no large plateaux are present, a fine vertical resolution can be maintained in this way in most of the boundary layer. At the same time, all the necessary upper grid layers can be included with limited computational overhead.

2. THE NONHYDROSTATIC MODEL EQUATIONS

The Reynolds averaged equations for a dry, fully compressible atmosphere can be written in advection form as

$$\begin{aligned} &\frac{d\log\rho}{dt} + \nabla\cdot\mathbf{v} = 0 \\ &\frac{d\mathbf{v}}{dt} + \mathbf{F}\mathbf{v} = -c_p\theta\nabla\pi - g\mathbf{k} + \mu\Delta\mathbf{v} + \frac{\partial}{\partial z}\left(\nu\frac{\partial\mathbf{v}}{\partial z}\right) \\ &\frac{d\theta}{dt} = \mu\Delta\theta + \frac{\partial}{\partial z}\left(\nu\frac{\partial\theta}{\partial z}\right) + Q_\theta. \end{aligned} \tag{1}$$

Here, Cartesian (x, y, z) coordinates have been used, the velocity field is given by $\mathbf{v} = (u, v, w)$, $\mathbf{k} = (0, 0, 1)$ denotes the vertical direction, and

$$\frac{d}{dt} = \frac{\partial}{\partial t} + \mathbf{v}\cdot\nabla \tag{2}$$

is the Lagrangian derivative. Furthermore, π will denote the Exner pressure function, T is the absolute temperature, ρ is the density, R is the ideal gas constant, c_p, c_v are, respectively, the constant pressure and constant volume specific heats of dry air, and p_0 is a reference

pressure value. The thermodynamic variables for an ideal gas can then be defined as

$$\pi = \left(\frac{p}{p_0}\right)^{\kappa}, \qquad \theta = \frac{T}{\pi}, \qquad \rho = \frac{p_0 \pi^{\frac{c_v}{R}}}{R\theta}, \qquad \kappa = \frac{R}{c_p}, \qquad \frac{1}{\kappa} - 1 = \frac{c_v}{R}. \tag{3}$$

The turbulent viscosity coefficients μ, ν are assumed to be known nonnegative functions of the flow field and thermodynamic variables. The Coriolis acceleration coefficients are assumed to be constant and are written in matrix form as

$$\mathbf{F} = \begin{bmatrix} 0 & -f & 0 \\ f & 0 & 0 \\ 0 & 0 & 0 \end{bmatrix}.$$

Since

$$\log \rho = \frac{c_v}{R} \log \pi - \log \theta + \log \frac{p_0}{R},$$

Eqs. (1) can then be rewritten as

$$\begin{aligned} \frac{d \log \pi}{dt} + \frac{R}{c_v} \nabla \cdot \mathbf{v} &= \frac{R}{c_v} \frac{d \log \theta}{dt} \\ \frac{d\mathbf{v}}{dt} + \mathbf{F}\mathbf{v} &= -c_p \theta \nabla \pi - g\mathbf{k} + \mu \Delta \mathbf{v} + \frac{\partial}{\partial z}\left(\nu \frac{\partial \mathbf{v}}{\partial z}\right) \\ \frac{d\theta}{dt} &= \mu \Delta \theta + \frac{\partial}{\partial z}\left(\nu \frac{\partial \theta}{\partial z}\right) + Q_\theta. \end{aligned} \tag{4}$$

The numerical scheme presented in this paper only deals with the inviscid and adiabatic case. Therefore, turbulent viscosities and diabatic heating will be omitted in what follows. Reference profiles of Exner pressure $\Pi = \Pi(z)$ and potential temperature $\Theta = \Theta(z)$ which are assumed to represent a stably stratified, hydrostatic atmosphere are then introduced for convenience, so that $\pi = \Pi + \tilde{\pi}$, $\frac{d\Theta}{dz} > 0$, and

$$c_p \Theta \frac{d\Pi}{dz} = -g. \tag{5}$$

θ will denote from now on the deviation from the profile Θ, thus yielding the model equations

$$\frac{d \log(\Pi + \tilde{\pi})}{dt} + \frac{R}{c_v} \nabla \cdot \mathbf{v} = 0 \tag{6}$$

$$\frac{d\mathbf{v}}{dt} + \mathbf{F}\mathbf{v} = -c_p(\Theta + \theta)\nabla(\Pi + \tilde{\pi}) - g\mathbf{k} \tag{7}$$

$$\frac{d\theta}{dt} + w \frac{d\Theta}{dz} = 0. \tag{8}$$

In order to avoid cancellation of almost equal terms, the equation for the vertical velocity is then rewritten as

$$\frac{dw}{dt} = -c_p \Theta \frac{\partial \tilde{\pi}}{\partial z} + g \frac{\theta}{\Theta} - c_p \theta \frac{\partial \tilde{\pi}}{\partial z}. \tag{9}$$

It should be noticed that, although it is in fact possible to linearize Eq. (6) around the reference pressure profile, so as to obtain a linear equation for $\tilde{\pi}$, the nonlinear equation is retained here. In this way, the resulting model is much less dependent on the reference profile chosen. Furthermore, in the context of a semi-implicit discretization approach, the term $w\frac{d\log\Pi}{dz}$ which arises in the linearization would yield a further, undesired coupling between the pressure and vertical velocity equations.

The formulation of appropriate boundary conditions for atmospheric models is a widely debated problem for which only partial solutions exist (see, e.g., [15, 27, 30, 37]). For the purposes of the present implementation, an absorbing layer (see [28] for a detailed description) will be employed at the upper and lateral boundaries in order to avoid reflection of outgoing waves. For the elliptic equation which the semi-implicit discretization will yield for the nonhydrostatic pressure $\tilde{\pi}$, a Neumann boundary condition will be imposed. At the lower boundary, the velocity component normal to the boundary is taken to be zero, and a Neumann condition of zero flux will be imposed for all other variables. As it will be clear in the following section, the proposed boundary discretization results in a step mountain approximation of the orographic profile, so that the velocity component normal to the boundary coincides with either u, v, or w.

3. COMPUTATIONAL DOMAIN AND GRID ARRANGEMENT

The equations are considered on the domain

$$\mathcal{D} = \{(x, y, z) : (x, y) \in [0, L_x] \times [0, L_y], h(x, y) \le z \le L_z\},$$

where h is some representation of the orographic profile. A staggered discretization grid with at most $N_x \times N_y \times N_z$ computational cells is introduced. The horizontal grid spacings are assumed to be constant for simplicity and are defined as $\Delta x = L_x/N_x$, $\Delta y = L_y/N_y$. However, the model has also been implemented on stretched horizontal grids without substantial modification of the discretization approach. Let then $\tilde{z}_{k-1/2}$ denote the height above mean sea level of the lower face of cell k and $\tilde{z}_k$ the height above mean sea level of the center of cell k, for $k = 1, \ldots, N_z + 1$. The vertical grid spacings are defined by $\Delta\tilde{z}_k = \tilde{z}_{k+1/2} - \tilde{z}_{k-1/2}$, for $k = 1, \ldots, N_z$.

Only the cells above the Earth's surface belong to the effective computational domain. Bottom cells are denoted for each i, j by the indexes $k = m_{i,j}$. Specifically,

$$m_{i,j} = \min_{1\le k\le N_z}\left\{k: h_{i,j} < \tilde{z}_{k+\frac{1}{2}}\right\}.$$

Dependency of such indexes on i, j is often omitted for clarity in what follows. Furthermore, heights of the cell faces above orography are introduced for each i, j and for $k = m_{i,j}, \ldots, N_z$. These will in general depend on i, j, k and can be defined as

$$\Delta z_{i+\frac{1}{2},j,k} = \begin{cases} \max\left(\tilde{z}_{k+\frac{1}{2}} - h_{i+\frac{1}{2},j}, 0\right) & \text{for } k = m_{i+1.j} \text{ and } k = m_{i,j} \\ \Delta z_{i+\frac{1}{2},j,k} = \Delta\tilde{z}_k & \text{otherwise} \end{cases}$$

$$\Delta z_{i,j,k} = \max\left(\Delta z_{i+\frac{1}{2},j,k}, \Delta z_{i-\frac{1}{2},j,k}, \Delta z_{i,j+\frac{1}{2},k}, \Delta z_{i,j-\frac{1}{2},k}\right).$$

Top and bottom cells will be assumed of rectangular shape with horizontal dimensions Δx, Δy and vertical dimension $\Delta z_{i,j,k}$. Each cell is numbered at its center with indices i, j,

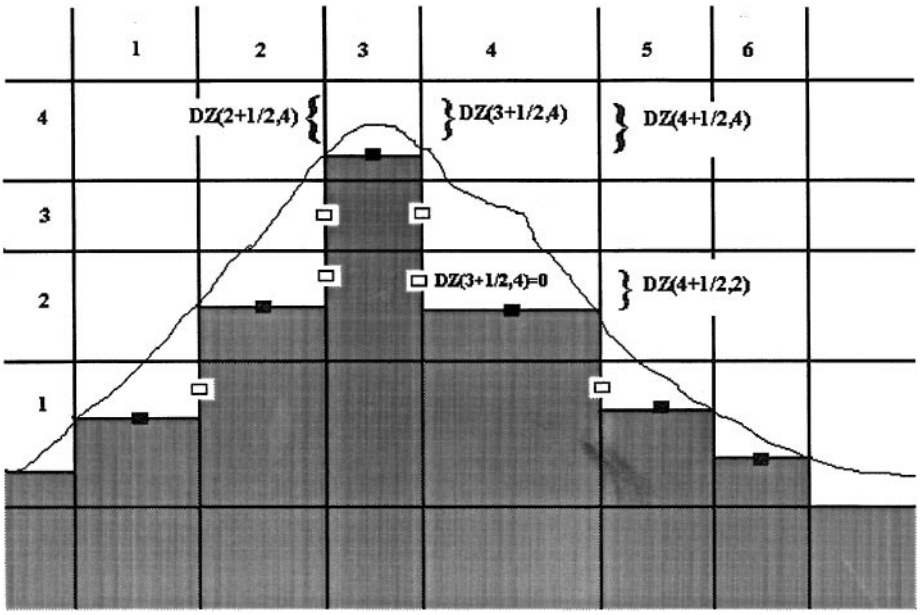

FIG. 1. Vertical section of the computational grid.

and k. The discrete u velocity is defined at half integer i and integers j and k; v is defined at integers i, k, and half integer j; while w, θ, and Θ are defined at integers i, j, and half integers k. Orography profile heights are defined both at u and v locations. Finally, π and all other three-dimensional scalar variables are defined at integers i, j, k. At points where they are not defined, the discrete variables are generally computed by simple arithmetical mean of the nearest defined values.

An example of the vertical section of such a computational grid is shown in Fig. 1, together with the corresponding idealized orography profile. It can be observed that, for example, $\Delta z_{2+1/2,4}$, $\Delta z_{3+1/2,4}$ take different values, as well as $\Delta z_{3+1/2,4}$, $\Delta z_{4+1/2,4}$, and $\Delta z_{3+1/2,2}$, $\Delta z_{4+1/2,2}$, respectively. Furthermore, $\Delta z_{3,4} = \Delta z_{2+1/2,4}$, and $\Delta z_{4,4} = \Delta z_{4+1/2,4}$. Vertical walls are taken into account by assuming the corresponding $\Delta z_{i+1/2,j,k}$ to be zero. For example, in the grid shown in Fig. 1, $\Delta z_{3+1/2,2} = 0$, as well as $\Delta z_{3+1/2,3}$, $\Delta z_{2+1/2,2}$, and $\Delta z_{2+1/2,3}$. Furthermore, the small black squares denote gridpoints where the boundary condition $w = 0$ is imposed, while the small white squares denote gridpoints where the boundary condition $u = 0$ is imposed. The grid which is built in this way is different from those of the so-called *shaved cell* approaches (see, e.g., [1]), since the orographic profile is in fact approximated by a step mountain. However, sufficient accuracy will be achieved by the finite volume discretization of Eq. (6). Such discretization is performed by assuming no contribution to the flux of the areas below orography on each face, thus accounting for the different heights at the cell faces. It is also to be remarked that in this discretization of the lower boundary, velocity components normal to the boundary coincide with either u, v, or w values, so that imposing the appropriate boundary condition on velocity is rather straightforward. Difference operators are then introduced as

$$\delta_x \phi_{i+\frac{1}{2},j,k} = \frac{\phi_{i+1,j,k} - \phi_{i,j,k}}{\Delta x}, \qquad \delta_y \phi_{i,j+\frac{1}{2},k} = \frac{\phi_{i,j+1,k} - \phi_{i,j,k}}{\Delta y}$$

$$\delta_z \phi_{i,j,k+\frac{1}{2}} = \frac{\phi_{i,j,k+1} - \phi_{i,j,k}}{\Delta z_{i,j,k+\frac{1}{2}}}$$

for variables defined at the cell centers and as

$$\delta_x \phi_{i,j,k} = \frac{\phi_{i+\frac{1}{2},j,k} - \phi_{i-\frac{1}{2},j,k}}{\Delta x}, \qquad \delta_y \phi_{i,j,k} = \frac{\phi_{i,j+\frac{1}{2},k} - \phi_{i,j-\frac{1}{2},k}}{\Delta y}$$

$$\delta_z \phi_{i,j,k} = \frac{\phi_{i,j,k+\frac{1}{2}} - \phi_{i,j,k-\frac{1}{2}}}{\Delta z_{i,j,k}}$$

for variables defined at the cell sides. A discrete divergence operator is also defined as

$$\mathrm{div}(u, v, w)_{i,j,k} = \frac{1}{\Delta z_{i,j,k}} \left[\frac{\Delta z_{i+\frac{1}{2},j,k} u_{i+\frac{1}{2},j,k} - \Delta z_{i-\frac{1}{2},j,k} u_{i-\frac{1}{2},j,k}}{\Delta x} + \frac{\Delta z_{i,j+\frac{1}{2},k} v_{i,j+\frac{1}{2},k} - \Delta z_{i,j-\frac{1}{2},k} v_{i,j-\frac{1}{2},k}}{\Delta y} + w_{i,j,k+\frac{1}{2}} - w_{i,j,k-\frac{1}{2}} \right].$$

4. A SEMI-IMPLICIT AND SEMI-LAGRANGIAN SOLUTION ALGORITHM

A semi-implicit, semi-lagrangian discretization scheme is now introduced. In order to obtain a scheme whose stability is independent of the sound wave speed, the gradient of the Exner pressure function in the momentum equations and the velocity divergence in the continuity equation are discretized implicitly in time. A coupling is also to be maintained between the buoyancy term in the w equation and the vertical advection term in the equation for θ. Furthermore, for simplification of the resulting algebraic system, the terms $c_p\theta \frac{\partial \pi}{\partial x}$, $c_p\theta \frac{\partial \pi}{\partial y}$ in the horizontal momentum equations and the term $c_p\theta \frac{\partial \tilde{\pi}}{\partial z}$ in the vertical momentum equation are discretized explicitly in time (see also [9, 10, 28, 42]). This relies on the implicit assumption that θ is not too large with respect to Θ, somewhat in the spirit of the classical Boussinesq approximation, so that no severe stability restrictions on the discretization timestep result. The discretization of Eqs. (6)–(9) at the internal nodes is then given by

$$\log\left(1 + \frac{\tilde{\pi}^{n+1}_{i,j,k}}{\Pi_k}\right) + \frac{\alpha R}{c_v} \mathrm{div}(u^{n+1}, v^{n+1}, w^{n+1})_{i,j,k} \Delta t = (\mathcal{G}\pi)^n_{i,j,k} \tag{10}$$

$$u^{n+1}_{i+\frac{1}{2},j,k} + \alpha c_p \Theta_k \delta_x \tilde{\pi}^{n+1}_{i+\frac{1}{2},j,k} \Delta t = (\mathcal{G}u)^n_{i+\frac{1}{2},j,k} \tag{11}$$

$$v^{n+1}_{i,j+\frac{1}{2},k} + \alpha c_p \Theta_k \delta_y \tilde{\pi}^{n+1}_{i,j+\frac{1}{2},k} \Delta t = (\mathcal{G}v)^n_{i,j+\frac{1}{2},k} \tag{12}$$

$$w^{n+1}_{i,j,k+\frac{1}{2}} - g\alpha \frac{\theta^{n+1}_{i,j,k+\frac{1}{2}}}{\Theta_{k+\frac{1}{2}}} \Delta t + \alpha c_p \Theta_{k+\frac{1}{2}} \delta_z \tilde{\pi}^{n+1}_{i,j,k+\frac{1}{2}} \Delta t = (\mathcal{G}w)^n_{i,j,k+\frac{1}{2}} \tag{13}$$

$$\theta^{n+1}_{i,j,k+\frac{1}{2}} + \alpha \left.\frac{d\Theta}{dz}\right|_{k+\frac{1}{2}} w^{n+1}_{i,j,k+\frac{1}{2}} \Delta t = (\mathcal{G}\theta)^n_{i,j,k+\frac{1}{2}}, \tag{14}$$

where the right hand side terms are defined, respectively, as

$$(\mathcal{G}\pi)^n_{i,j,k} = \mathcal{L}(\log \pi)^n_{i,j,k} - \log(\Pi_k) - \frac{(1-\alpha)R}{c_v} \mathcal{L}\,\mathrm{div}(u^n, v^n, w^n)_{i,j,k} \Delta t$$

$$(\mathcal{G}u)^n_{i+\frac{1}{2},j,k} = \mathcal{L}(u - (1-\alpha)c_p \Theta \delta_x \tilde{\pi}\,\Delta t - c_p \theta \delta_x \tilde{\pi}\,\Delta t)^n_{i+\frac{1}{2},j,k}$$

$$(\mathcal{G}v)^n_{i,j+\frac{1}{2},k} = \mathcal{L}(v - (1-\alpha)c_p\Theta\delta_y\tilde{\pi}\,\Delta t - c_p\theta\delta_y\tilde{\pi}\,\Delta t)^n_{i,j+\frac{1}{2},k}$$

$$(\mathcal{G}w)^n_{i,j,k+\frac{1}{2}} = \mathcal{L}\left(w - (1-\alpha)c_p\Theta\delta_z\tilde{\pi}\,\Delta t - c_p\theta\delta_z\tilde{\pi}\,\Delta t + g(1-\alpha)\frac{\theta}{\Theta}\Delta t\right)^n_{i,j,k+\frac{1}{2}}$$

$$(\mathcal{G}\theta)^n_{i,j,k+\frac{1}{2}} = \mathcal{L}\left(\theta - (1-\alpha)\frac{d\Theta}{dz}w\Delta t\right)^n_{i,j,k+\frac{1}{2}}.$$

It is to be remarked that, due to the definition of the pressure values at the center of each computational cell, the approximation of the horizontal pressure gradients is generally only first order accurate in the bottom cells where $k = m_{i,j}$. Here the symbol $\mathcal{L}$ denotes the interpolation at the departure point of the lagrangian trajectory ending in $(i\Delta x, j\Delta y, k\Delta z)$ at time $(n+1)\Delta t$ (see, e.g., [36]). As it is easily seen, a first order average along the trajectory has been employed for the semi-lagrangian time discretization, where one must require $\alpha \in [\frac{1}{2}, 1]$ for stability. Higher order averages could also be considered (see, e.g., [31]). In the present implementation, bicubic Lagrange interpolation has been used at the trajectory departure point. In the three lowermost cells above orography, bilinear interpolation is used. The trajectories are computed by an explicit second order Runge–Kutta method, which is applied to each trajectory with a timestep that is an appropriate fraction of Δt depending on the local Courant number, so as to avoid crossing of the computed characteristics (this substepping algorithm is described in detail in [3, 7]). In the trajectory computation, wind components are extrapolated at time $n+\frac{1}{2}$. As a result of the substepping algorithm employed, all the trajectory departure points lie in the computational domain.

Furthermore, the discretization of the Coriolis terms has been omitted here for simplicity of the presentation. They can be easily included by a semi-implicit operator splitting approach, which, although inadequate for synoptic scale applications (see, e.g., [44]), is sufficiently accurate for simulation of mesoscale flows. It is then to be remarked that, in the finite volume discretization of Eq. (6) given by Eq. (10), the normal velocity on the areas of each face below orography has been taken to be zero, thus accounting for the varying orographic height at the cells faces. As a result of the orography approximation, the normal derivatives at the boundary coincide with the derivatives with respect to x, y, and z, respectively. Therefore, imposing zero flux boundary conditions on $\tilde{\pi}$ and θ is quite straightforward, as well as imposing the free slip boundary condition on the staggered velocity components.

Substitution of Eq. (14) into Eq. (13) is now performed, to obtain

$$w^{n+1}_{i,j,k+\frac{1}{2}} = A_{k+\frac{1}{2}}(\mathcal{G}w)^n_{i,j,k+\frac{1}{2}} - \alpha c_p A_{k+\frac{1}{2}}\Theta_{k+\frac{1}{2}}\delta_z\tilde{\pi}^{n+1}_{i,j,k+\frac{1}{2}}\Delta t, \tag{15}$$

where

$$A_{k+\frac{1}{2}} = \left(1 + g\frac{\alpha^2\Delta t^2}{\Theta_{k+\frac{1}{2}}}\left.\frac{d\Theta}{dz}\right|_{k+\frac{1}{2}}\right)^{-1}$$

and where $(\mathcal{G}w)^n_{i,j,k+1/2}$ has now been redefined as

$$(\mathcal{G}w)^n_{i,j,k+\frac{1}{2}} = \mathcal{L}\left(w - (1-\alpha)c_p\Theta\delta_z\tilde{\pi}\,\Delta t - c_p\theta\delta_z\tilde{\pi}\,\Delta t + g(1-\alpha)\frac{\theta}{\Theta}\Delta t\right)^n_{i,j,k+\frac{1}{2}}$$
$$+ \alpha\frac{g}{\Theta_{k+\frac{1}{2}}}(\mathcal{G}\theta)^n_{i,j,k+\frac{1}{2}}\Delta t.$$

Substitution of the discrete Eqs. (11), (12), and (13) into Eq. (10) yields then

$$\log\left(1+\frac{\tilde{\pi}^{n+1}_{i,j,k}}{\Pi_k}\right)-\alpha^2\frac{\Delta t^2 R c_p}{c_v}\,\mathrm{div}\big(\Theta\delta_x\tilde{\pi}^{n+1},\,\Theta\delta_y\tilde{\pi}^{n+1},\,A\Theta\delta_z\tilde{\pi}^{n+1}\big)_{i,j,k}=\psi^n_{i,j,k},\quad(16)$$

where

$$\psi^n_{i,j,k}=(\mathcal{G}\pi)^n_{i,j,k}-\frac{\alpha R}{c_v}\,\mathrm{div}((\mathcal{G}u)^n,\,(\mathcal{G}v)^n,\,A(\mathcal{G}w^n))_{i,j,k}\Delta t.$$

For each i, j, k, Eq. (16) can be rewritten as

$$\begin{aligned}&\Delta z_{i,j,k}\log\left(1+\frac{\tilde{\pi}^{n+1}_{i,j,k}}{\Pi_k}\right)\\&\quad+\left[a^n_{i+\frac12,j,k}+a^n_{i-\frac12,j,k}+b^n_{i,j+\frac12,k}+b^n_{i,j-\frac12,k}+c^n_{i,j,k+\frac12}+c^n_{i,j,k-\frac12}\right]\tilde{\pi}^{n+1}_{i,j,k}\\&\quad-a^n_{i+\frac12,j,k}\tilde{\pi}^{n+1}_{i+1,j,k}-a^n_{i-\frac12,j,k}\tilde{\pi}^{n+1}_{i-1,j,k}-b^n_{i,j+\frac12,k}\tilde{\pi}^{n+1}_{i,j+1,k}-b^n_{i,j-\frac12,k}\tilde{\pi}^{n+1}_{i,j-1,k}\\&\quad-c^n_{i,j,k+\frac12}\tilde{\pi}^{n+1}_{i,j,k+1}-c^n_{i,j,k-\frac12}\tilde{\pi}^{n+1}_{i,j,k-1}=\Delta z_{i,j,k}\psi^n_{i,j,k},\end{aligned}\quad(17)$$

where

$$a^n_{i+\frac12,j,k}=\alpha^2\frac{c_pR\Delta t^2}{c_v\Delta x^2}\Delta z^n_{i+\frac12,j,k}\Theta_k$$

$$b^n_{i,j+\frac12,k}=\alpha^2\frac{c_pR\Delta t^2}{c_v\Delta y^2}\Delta z^n_{i,j+\frac12,k}\Theta_k$$

$$c^n_{i,j,k+\frac12}=\alpha^2\frac{c_pR\Delta t^2}{c_v\Delta z_{i,j,k+\frac12}}A_{k+\frac12}\Theta_{k+\frac12}.$$

After the solution of the nonlinear system given by (17), the values of the velocities at time $n+1$ are updated with the implicit corrections to the pressure gradient, and the value of potential temperature at time $n+1$ is computed by Eq. (14).

For $i=1,\dots,N_x$, $j=1,\dots,N_y$, and $k=m_{i,j},\dots,N_z$, Eqs. (17) constitute a weakly nonlinear system of at most $N_x\times N_y\times N_z$ equations. As a consequence of the choice of the vertical coordinate z and of keeping the pressure equation in nonlinear form, the linear part of this system is given by a seven-diagonal, symmetric, and positive definite matrix, so that its solution can be computed, for example, by fixed point iteration based on the repeated application of the conjugate gradient method with simple preconditioning. It can be checked directly that arbitrarily complex orography and flow fields do not affect the good conditioning of the system. Since it can be shown in several test cases that no more than two nonlinear iterations are usually needed, a gain in efficiency is expected with respect to methods which require the solution of nonsymmetric systems. Furthermore, the simplification of the matrix structure is also expected to yield a greater efficiency of parallel implementations, by a diminished need for communication among processors.

5. CONVERGENCE OF THE NONLINEAR ITERATIONS

The numerical scheme introduced in the previous sections requires the solution of the large weakly nonlinear system (17) at each timestep. In order to solve efficiently such a system, it is convenient to define

$$d^n_{i,j,k} = \frac{\Delta z_{i,j,k}}{\Pi_k} + a^n_{i+\frac{1}{2},j,k} + a^n_{i-\frac{1}{2},j,k} + b^n_{i,j+\frac{1}{2},k} + b^n_{i,j-\frac{1}{2},k} + c^n_{i,j,k+\frac{1}{2}} + c^n_{i,j,k-\frac{1}{2}}$$

and

$$f_{i,j,k}\left(\tilde{\pi}^{n+1}_{i,j,k}\right) = \Delta z_{i,j,k}\left\{\log\left(1 + \frac{\tilde{\pi}^{n+1}_{i,j,k}}{\Pi_k}\right) - \frac{\tilde{\pi}^{n+1}_{i,j,k}}{\Pi_k}\right\}$$

so that Eq. (17) can be rewritten as

$$\begin{aligned} &f_{i,j,k}\left(\tilde{\pi}^{n+1}_{i,j,k}\right) + d^n_{i,j,k}\tilde{\pi}^{n+1}_{i,j,k} - a^n_{i+\frac{1}{2},j,k}\tilde{\pi}^{n+1}_{i+1,j,k} - a^n_{i-\frac{1}{2},j,k}\tilde{\pi}^{n+1}_{i-1,j,k} - b^n_{i,j+\frac{1}{2},k}\tilde{\pi}^{n+1}_{i,j+1,k} \\ &\quad - b^n_{i,j-\frac{1}{2},k}\tilde{\pi}^{n+1}_{i,j-1,k} - c^n_{i,j,k+\frac{1}{2}}\tilde{\pi}^{n+1}_{i,j,k+1} - c^n_{i,j,k-\frac{1}{2}}\tilde{\pi}^{n+1}_{i,j,k-1} = \Delta z_{i,j,k}\psi^n_{i,j,k}, \end{aligned} \tag{18}$$

where $i = 1, \ldots, N_x$, $j = 1, \ldots, N_y$, $k = m_{i,j}, \ldots, M_{i,j}$. Equations (18) constitute a nonlinear system of the form

$$\mathbf{f}(\mathbf{x}) + \mathbf{A}\mathbf{x} = \mathbf{b}, \tag{19}$$

where $\mathbf{A}$ is a seven-diagonal, symmetric, diagonally dominant matrix which can then be easily shown by the Gershgorin theorem (see, e.g., [39]) to be positive definite. $\mathbf{f}$, $\mathbf{x}$ are here vectors in $R^{N_x \times N_y \times N_z}$. The fixed point iterations defined by

$$\begin{aligned} \mathbf{x}^0 &= \text{initial guess obtained, e.g., from } \tilde{\pi}^n \\ \mathbf{A}\mathbf{x}^{k+1} &= \mathbf{b} - \mathbf{f}(\mathbf{x}^k) \end{aligned} \tag{20}$$

are easily proven to converge to the solution of (19), provided that

$$\|\mathbf{A}^{-1}\| \left\| \frac{\partial \mathbf{f}}{\partial \mathbf{x}} \right\| < 1,$$

where $\|\cdot\|$ denotes the matrix norm subordinate to the euclidean vector norm. The matrix valued function $\mathbf{H} = \frac{\partial \mathbf{f}}{\partial \mathbf{x}}$ is diagonal and is given componentwise by

$$h_{i,j,k}(\tilde{\pi}_{i,j,k}) = -\frac{\Delta z_{i,j,k}}{\Pi_k}\frac{\tilde{\pi}_{i,j,k}}{\Pi_k + \tilde{\pi}_{i,j,k}}.$$

It can then be checked directly that, for convergence to be assured, it is sufficient that $\Pi_k < \Delta z_{i,j,k}$ and $|\tilde{\pi}^n_{i,j,k}| < \Pi_k/2$. Considering that the nonhydrostatic correction is usually much smaller in value than the reference hydrostatic profile, and that the Exner pressure is usually normalized assuming $p_0 = 10^5$ Pa, this means that allowing a minimum $\Delta z_{i,j,k} = 2$ m will be sufficient to ensure convergence in realistic applications to large scale flows. Other

iteration procedures could be considered, such as the generalized Newton method, possibly leading to improved performance. However, it is to be remarked that in several test cases a single fixed point iteration is sufficient for each timestep. At each iteration, the linear system in (20) is to be solved, for example, by some number of preconditioned conjugate gradient iterations. Application of block tridiagonal preconditioning based on the discretization of the vertical derivatives terms, as suggested in [13, 14], yields a quite efficient solution algorithm. Furthermore, the tolerance used in the stopping criterion for the conjugate gradient is rescaled with the norm of the right hand side of the linear system (see, e.g., [29]). As a result, in several test cases as little as five iterations are required by the preconditioned conjugate gradient method.

6. NUMERICAL RESULTS FOR TWO-DIMENSIONAL FLOWS OVER OROGRAPHY

Equations (6)–(9) constitute in principle a complete model of the dry, inviscid, adiabatic atmospheric dynamics on all physical scales. However, the proposed discretization scheme is expected to yield the greatest advantages and to display maximum efficiency for mesoscale simulations. For this reason, the scheme has been tested on several cases of two-dimensional flows over orography, in order to compare the results with known analytical solutions or their asymptotic expansions (see, e.g., [19, 23–26] and references therein). An isothermal atmosphere with $T = 273$ K has generally been assumed, so that $N = 0.0187\ \mathrm{s}^{-1}$. Reference potential temperature is computed accordingly and the reference pressure profile is obtained from the discrete hydrostatic equation. The full nonlinear model was used in all the tests carried out. The time averaging parameter α has been given values in the range (0.51, 0.53). The tolerance parameters were set at $\epsilon = 10^{-7}$ for the fixed point iterations to solve the nonlinear system and at $\epsilon = 10^{-8}$ for the linear conjugate gradient iterations, but the tolerance for the conjugate gradient has always been rescaled with the norm of the right hand side as previously remarked.

As a preliminary test, the model has been run with zero initial velocities, pressure, and potential temperature perturbations over various steep orographic profiles, such as a 10,000-m high rectangular mountain. Various cell aspect ratios and reference temperature profiles were used. In all cases, no generation of spurious flows due to the presence of steep slopes has been observed.

Several standard tests have then been performed with a *versiera*[2] of Agnesi mountain profile given by

$$h(x) = \frac{h_0}{1 + ((x - x_0)/a)^2}, \qquad 0 \le x \le L,$$

where h_0, a are the maximum height and half-width of the mountain, respectively. The profile is centered at a point x_0 and L is the width of the computational domain. In all the tests $x_0 = \frac{L}{2}$. The parameter values used are the same as for the tests presented in [28] for another semi-implicit and semi-lagrangian model also based on the fully compressible equations. The reference horizontal Courant number is usually taken to be approximately 0.5. In all

[2] The straightforward translation of this old Italian word is *female devil* or *witch*. However, it is quite sure that early investigators of this curve such as Grandi and Agnesi used the word as a technical one, related to the geometric properties of the curve, see, e.g., [20, 26].

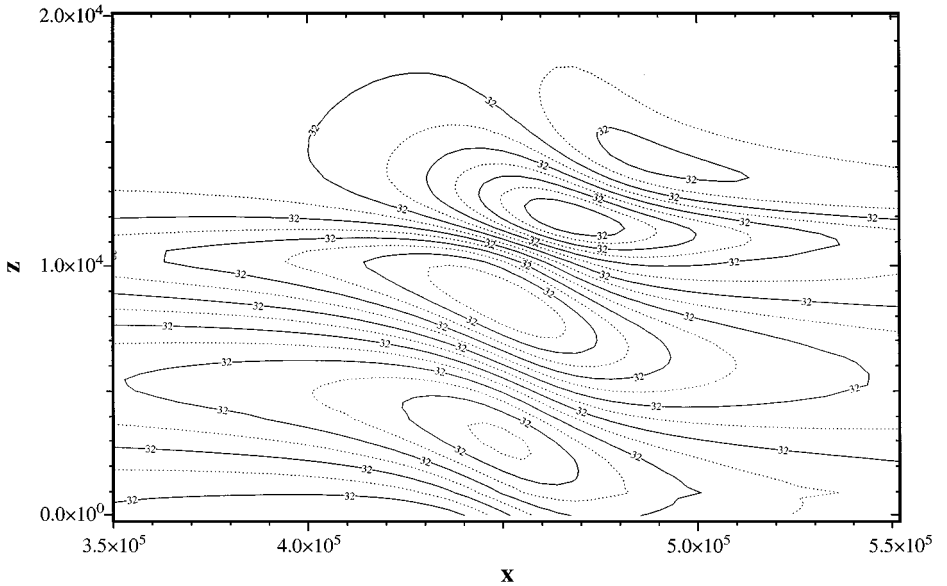

FIG. 2. Horizontal velocity in a linear hydrostatic stationary lee wave test case.

the tests, the orographic profile was inserted abruptly in the horizontally homogeneous flow at initial time.

A stationary test in the linear hydrostatic regime has been performed, i.e., with $\frac{aN}{U}$ much smaller than 1. More precisely, the model has been run with $a = 16$ km, $h_0 = 1$ m, at the resolution $\Delta x = 3$ km, $\Delta z = 250$ m. An initial horizontal velocity $U = 32$ m/s was prescribed. The horizontal velocity and the vertical velocity obtained at the rescaled time $t^* = \frac{Ut}{a} = 80$ with $\Delta t = 40$ s are plotted in Figs. 2, 3. The corresponding vertical momentum

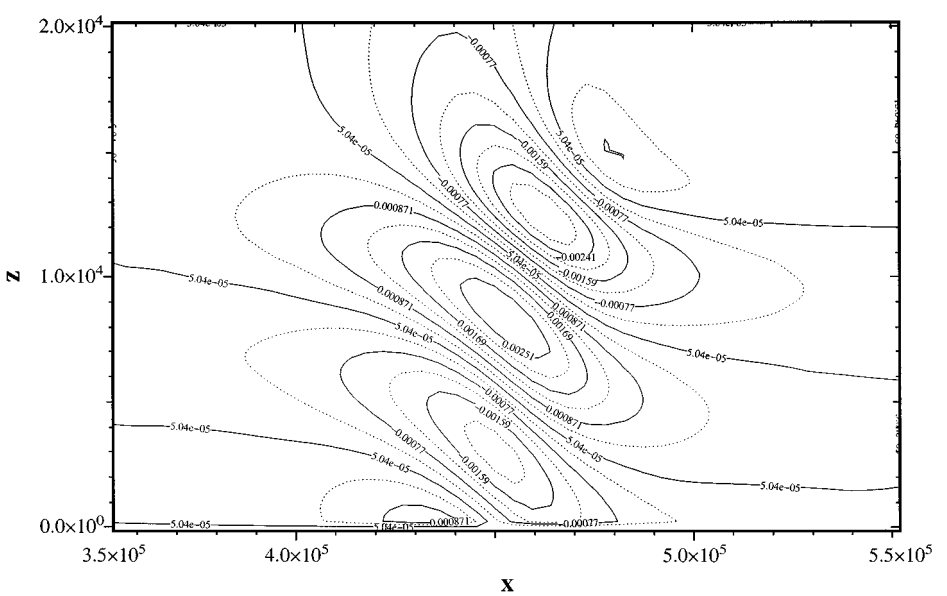

FIG. 3. Vertical velocity in a linear hydrostatic stationary lee wave test case.

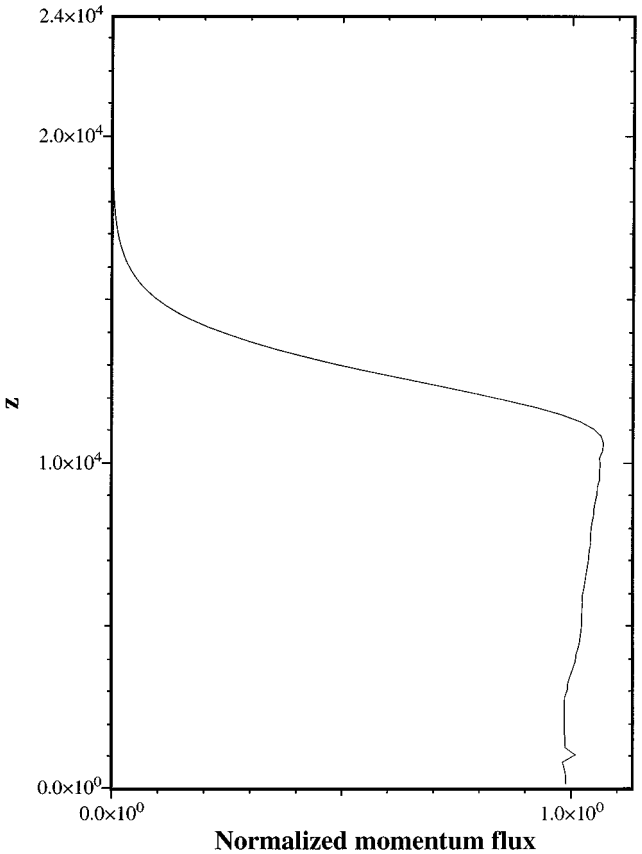

FIG. 4. Normalized vertical momentum flux in a linear hydrostatic stationary lee wave test case.

flux, normalized by its analytic value, is plotted in Fig. 4. It can be observed that the result is quite close to 1 throughout the undamped region below 10 km. A stationary test in the linear nonhydrostatic regime, i.e., with $\frac{aN}{U}$ of the order of 1, has been run with $a = 500$ m, $h_0 = 100$ m, at the resolution $\Delta x = 100$ m, $\Delta z = 250$ m. An initial horizontal velocity $U = 14$ m/s was prescribed. The vertical velocity obtained at the rescaled time $t^* = \frac{Ut}{a} = 120$ with $\Delta t = 4$ s is plotted in Fig. 5. The corresponding vertical momentum flux, normalized by the analytic linear hydrostatic value, is plotted in Fig. 6. It can be observed that the computed value is approximately 0.28, which can be compared with the analytic estimate of 0.3 for the nonhydrostatic case (see the references in [28]).

The linear time-dependent test case proposed in [34] was also performed. A potential temperature perturbation was placed at $x = 150$ km in a 400 km wide and 12 km high box without orography. An initial horizontal velocity $U = 20$ m/s was prescribed, and the spatial resolution used was $\Delta x = \Delta z = 1$ km. The contours of potential temperature perturbations at time $t = 3000$ s are shown in Fig. 7 and compare well with the structure displayed by the analytical solution. In this transient case, no more than 6 conjugate gradient iterations per timestep were necessary.

A nonlinear, hydrostatic stationary test has then been run assuming $a = 16$ km, $h_0 = 800$ m, at the resolution $\Delta x = 2.8$ km, $\Delta z = 200$ m and initial horizontal velocity $U = 32$ m/s. For this test case, temperature has been chosen so that $N = 0.02$ s^{-1}. The horizontal velocity,

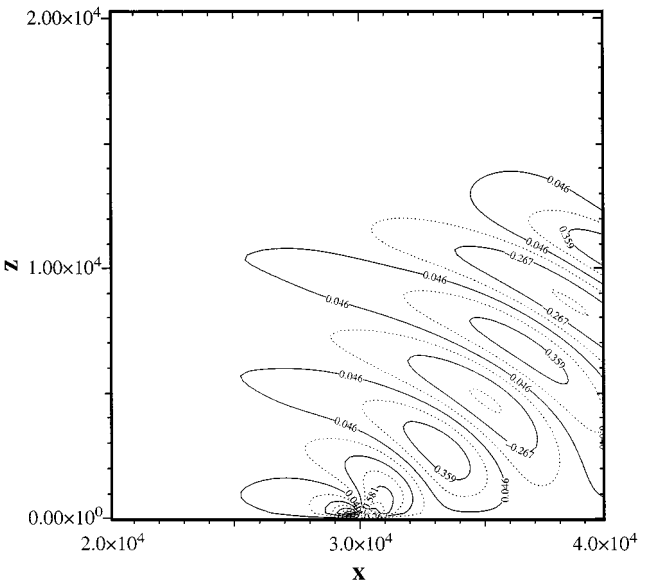

FIG. 5. Vertical velocity in a linear nonhydrostatic stationary lee wave test case.

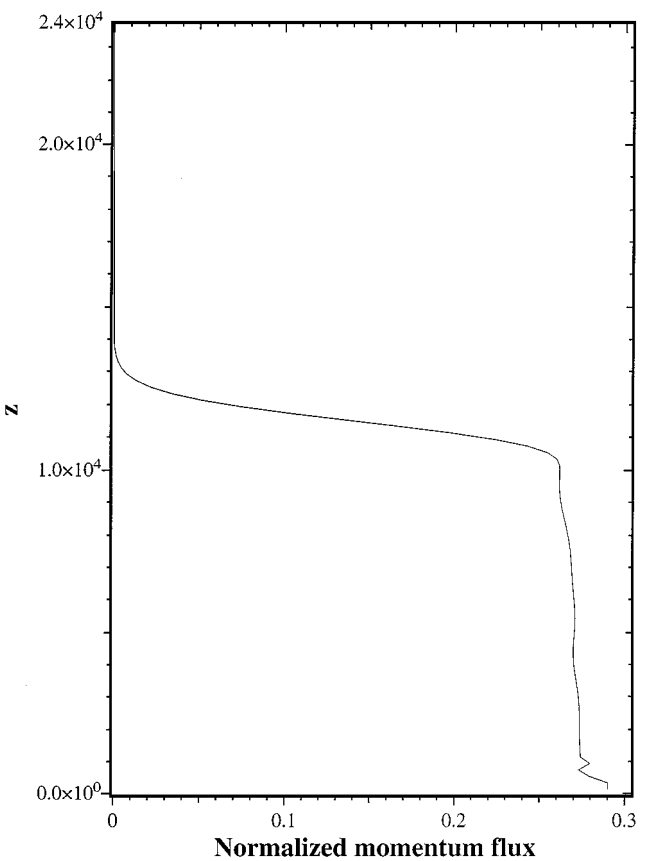

FIG. 6. Normalized vertical momentum flux in a linear nonhydrostatic stationary lee wave test case.

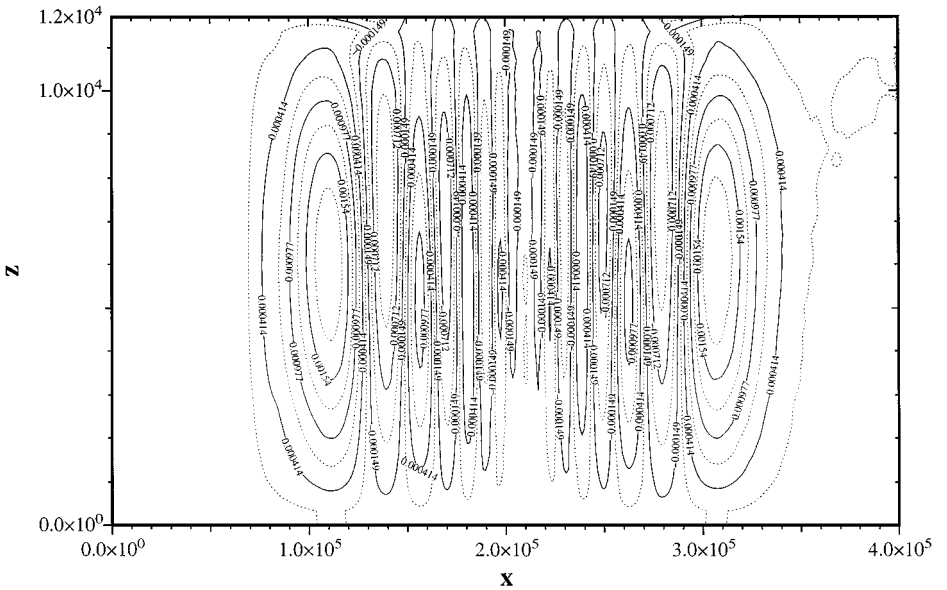

FIG. 7. Potential temperature perturbations in a linear nonhydrostatic time-dependent test case.

vertical velocity, and potential temperature contours obtained at the rescaled time $t^* = \frac{Ut}{a} = 172$ with $\Delta t = 30$ s are plotted in Figs. 8–10. It can be observed that the results agree well with those of [28]. The final steady state is reached quite slowly, but convergence to the analytical value of about 1.1 is clearly displayed in Fig. 11 (see again the references in [28]). A plot of the velocity field in this test case is also given in Fig. 12. In this type of plot, the vertical velocity component is rescaled and for each cell the velocity components have been interpolated linearly at the cell center. In order to show that the method also performs

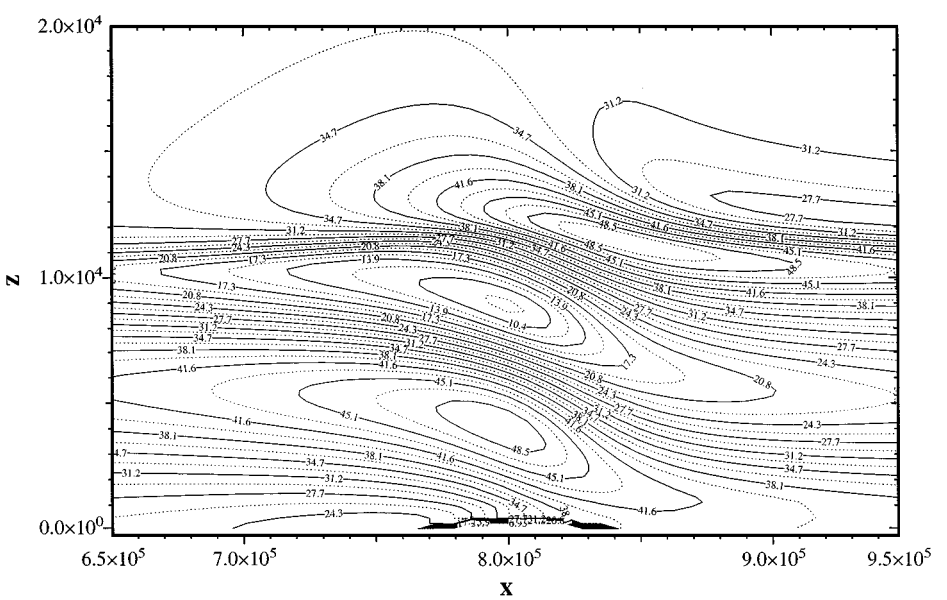

FIG. 8. Horizontal velocity in a nonlinear hydrostatic stationary lee wave test case.

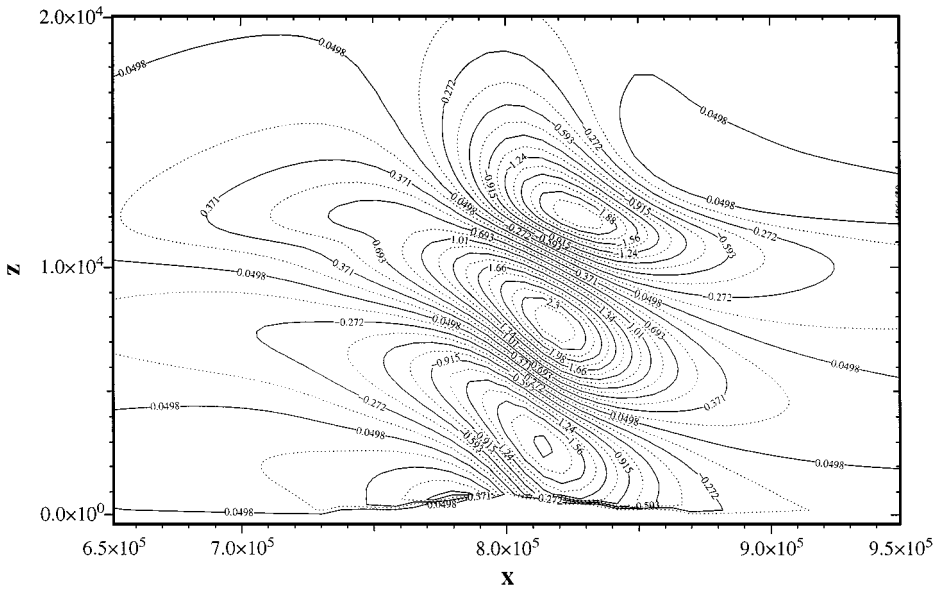

FIG. 9. Vertical velocity in a nonlinear hydrostatic stationary lee wave test case.

well when the mountain intersects a larger number of grid levels, a similar plot is shown in Fig. 13 for the same test case at the vertical resolution of 60 m.

Several nonlinear, nonhydrostatic regime stationary test cases have been run. In these tests, enough resolution had to be employed in order to reproduce steep orography profiles in a sufficiently accurate way on the computational grid described in Section 3. Otherwise, the approximated orography is too coarse and the computed flow stagnates or recirculates downsteam of the mountain where high vertical walls are present. Since the pressure gradient

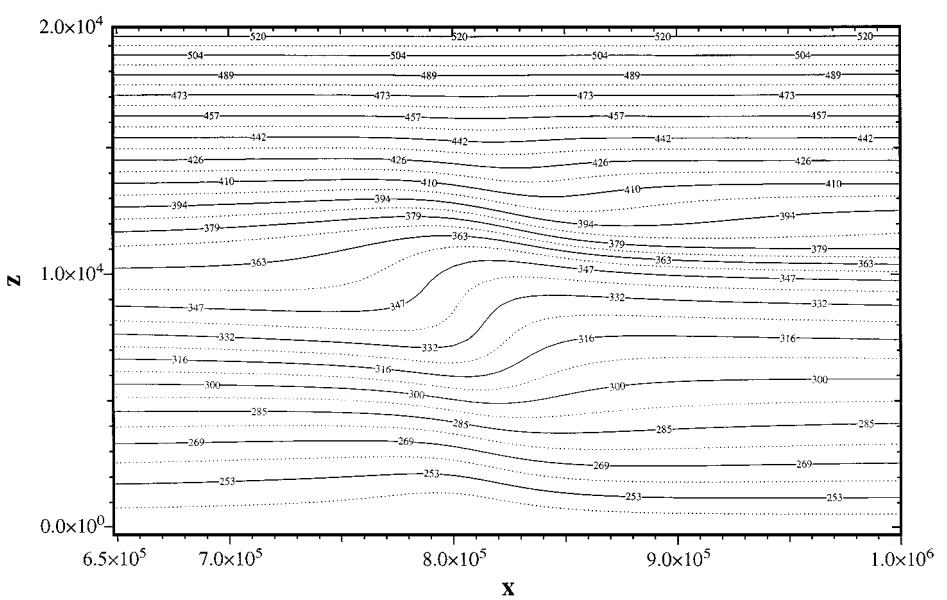

FIG. 10. Potential temperature in a linear hydrostatic lee wave test case.

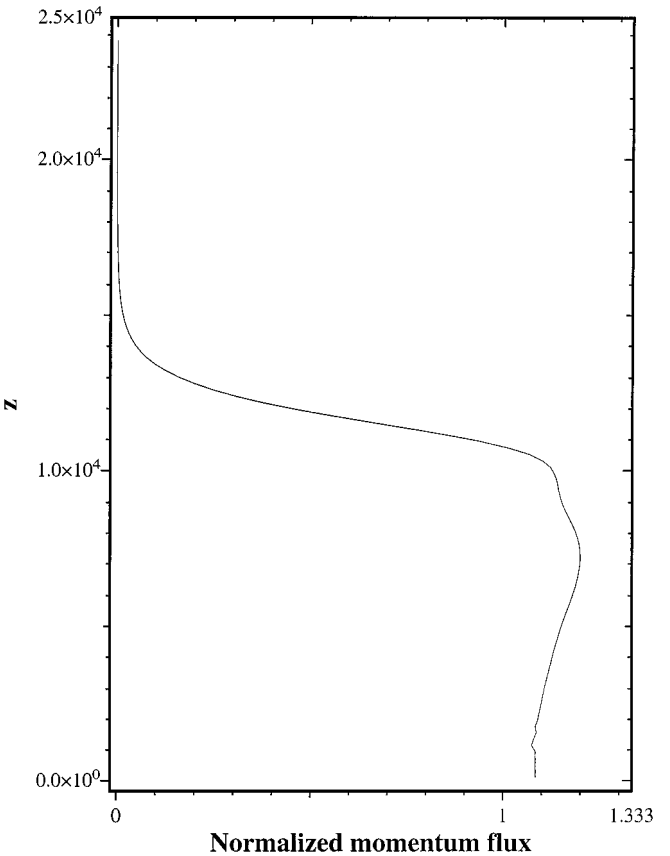

FIG. 11. Normalized vertical momentum flux profile in a nonlinear hydrostatic stationary lee wave test case.

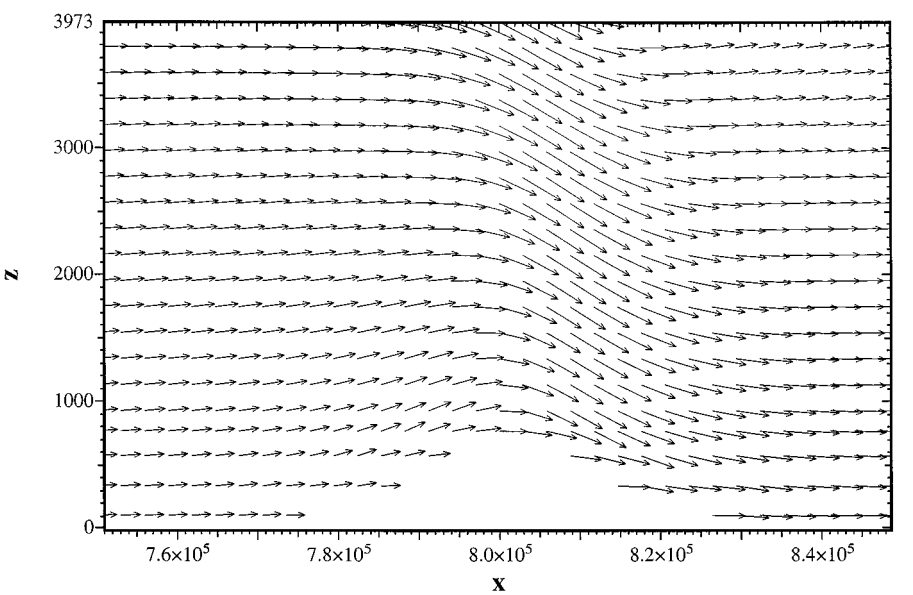

FIG. 12. Velocity field in a nonlinear hydrostatic lee wave test case.

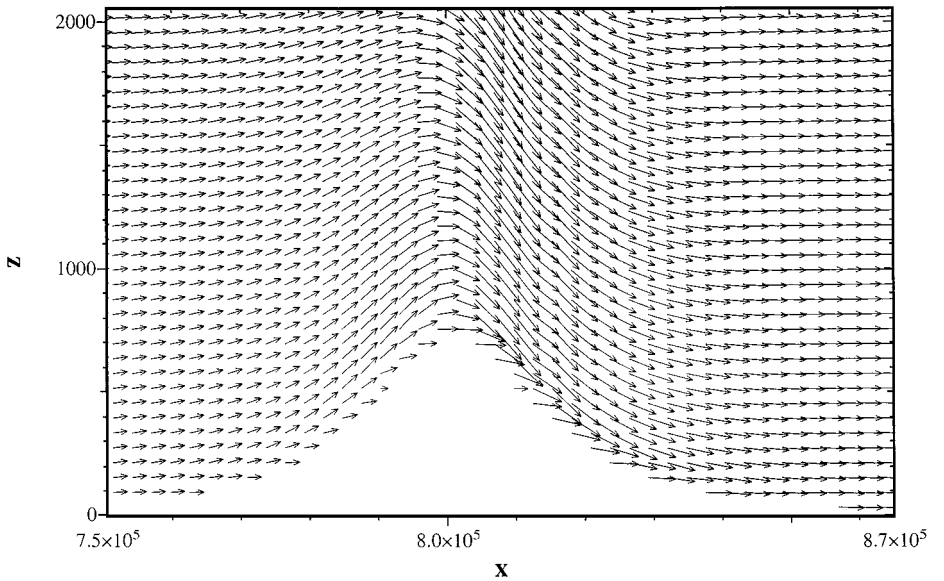

FIG. 13. Velocity field in a nonlinear hydrostatic lee wave test case run at vertical resolution $\Delta z = 60$ m.

terms are only first order accurate at the lowest model level, sufficient resolution is also necessary in order to keep this discretization error small. However, as it will be seen, the grid spacings required to obtain accurate results throughout the computational domain are realistic for high resolution simulations. Furthermore, even in the case of a coarse mountain description, the flow is always computed correctly above the top of the mountain.

A first test was performed with an Agnesi profile assuming $a = 1000$ m, $h_0 = 900$ m, so that the aspect ratio $\frac{h_0}{a} = 0.9$, at the resolution $\Delta x = 200$ m, $\Delta z = 100$ m and initial horizontal velocity $U = 13.28$ m/s. With these values of the parameters, the inverse Froude number $\frac{Na}{U}$ is about its critical value. The potential temperature, horizontal velocity, and vertical velocity contours obtained at time $t = 2400$ s with $\Delta t = 4$ s are plotted in Figs. 14–16. It can be observed that the steep wave pattern downstream of the obstacle is well

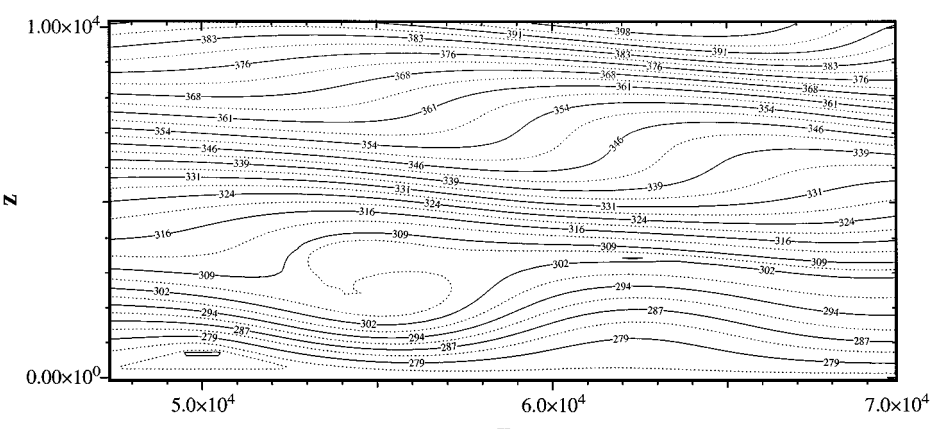

FIG. 14. Potential temperature in a nonlinear nonhydrostatic lee wave test case.

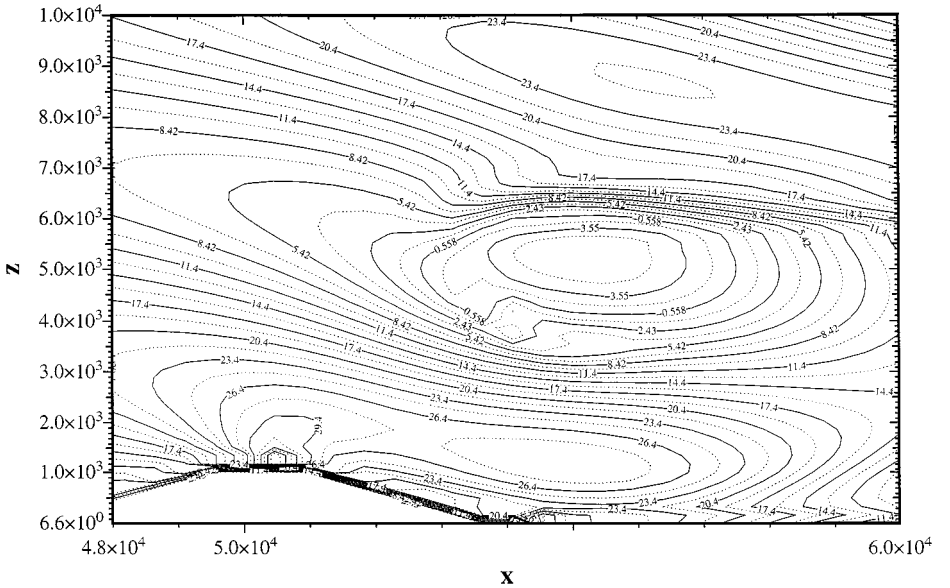

FIG. 15. Horizontal velocity in a nonlinear nonhydrostatic lee wave test case.

reproduced (see, e.g., the analytical solution presented in [24] for a similar case) and that the flow accelerates down the slope as expected. A plot of the typical velocity field in this test case is also given in Figs. 17 and 18 at various resolutions.

In order to test the performance of the model with even steeper orography, the same test was repeated with a 900-m high and 200-m wide rectangular mountain placed at $x = 45$ km at the resolution $\Delta x = 300$ m, $\Delta z = 100$ m. The potential temperature contours and velocity field obtained at time $t = 2500$ s with $\Delta t = 5$ s are plotted in Figs. 19–20. It is to be remarked

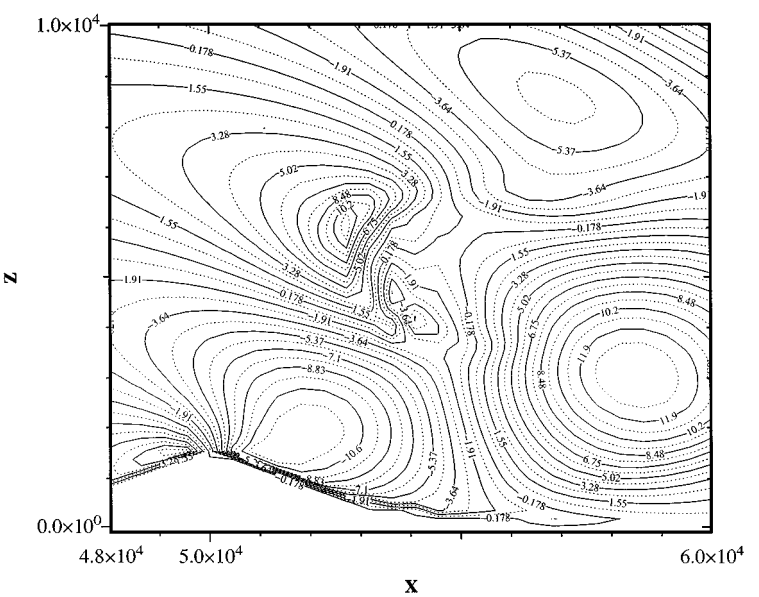

FIG. 16. Vertical velocity in a nonlinear nonhydrostatic lee wave test case.

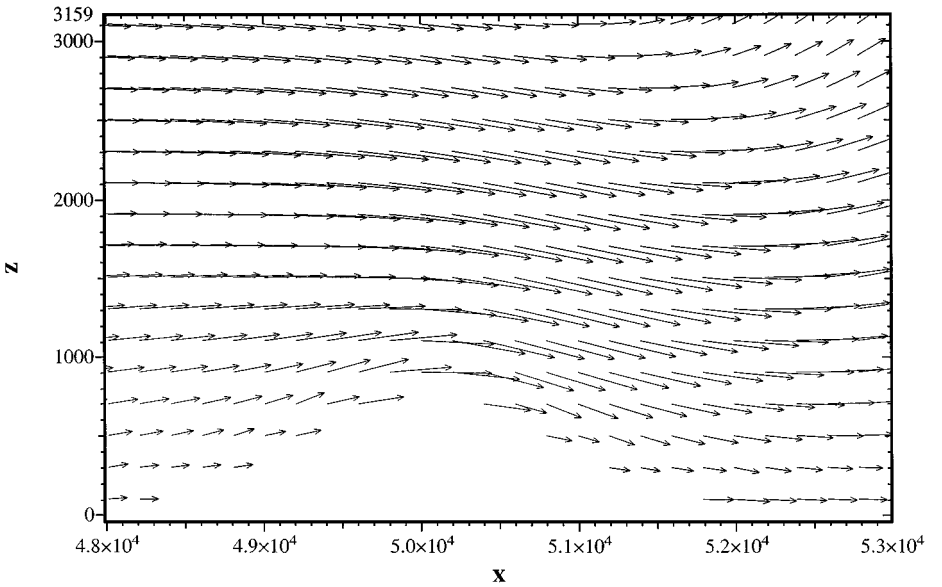

FIG. 17. Velocity field in a nonlinear nonhydrostatic lee wave test case run at resolution $\Delta x = \Delta z = 200$ m.

that the time step employed is 5 times that used in [28] in a similar steep orography test of the MC2 model. Furthermore, convergence of the iterative solver at each timestep was obtained with the same computational effort as in the case with smooth orography (no more than two nonlinear iterations which needed on average a total of about 10 preconditioned conjugate gradient iterations).

Finally, a nonlinear, nonhydrostatic time-dependent test was also run. The development of a warm bubble placed in an isentropic atmosphere at rest was studied, with parameters

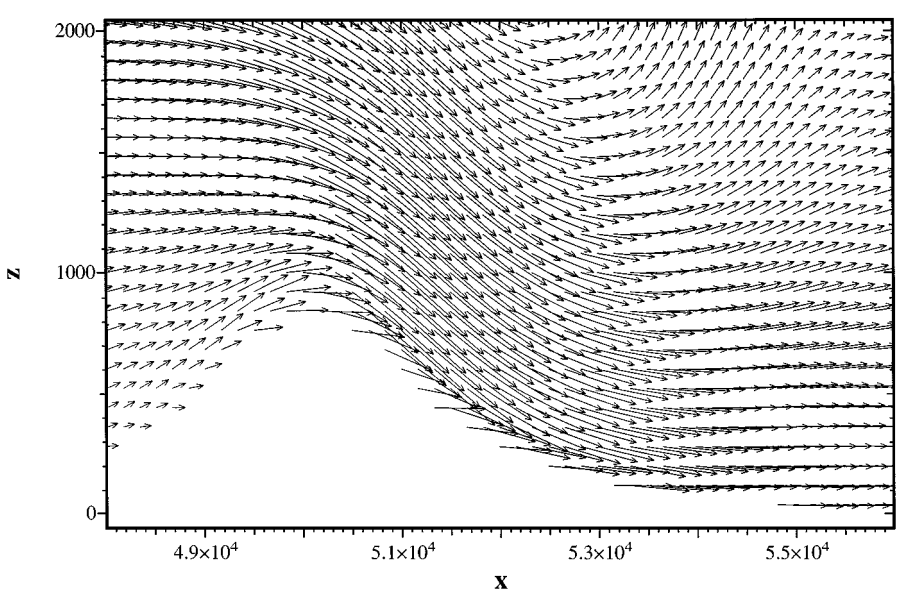

FIG. 18. Velocity field in a nonlinear nonhydrostatic lee wave test case run at resolution $\Delta x = 150$ m, $\Delta z = 80$ m.

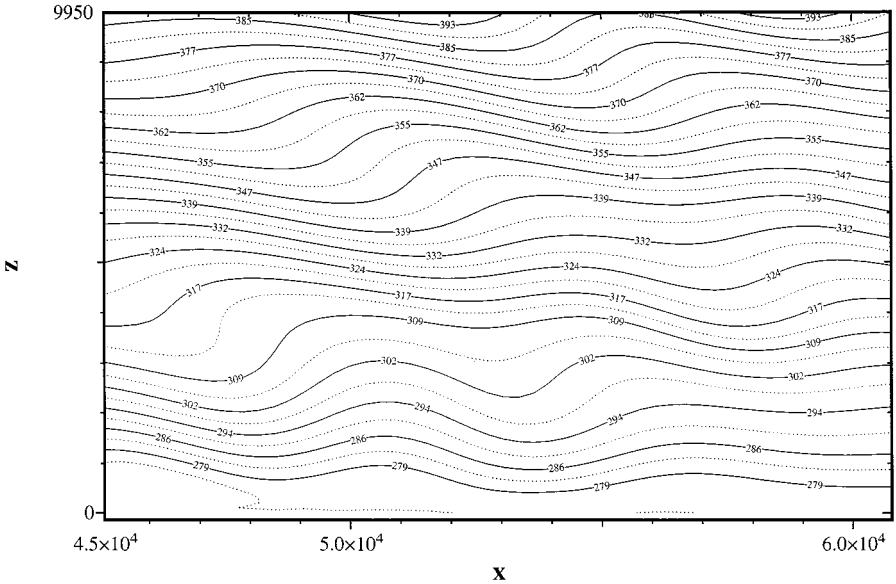

FIG. 19. Potential temperature in a flow over a thin rectangular obstacle.

analogous to those used in [8]. The potential temperature perturbation obtained at time 600 s with $\Delta t = 0.25$ s and a resolution of $\Delta x = \Delta z = 20$ m is shown in Fig. 21. No analytical solution is available in this case, but the computed results agree well with the corresponding reference numerical solution presented in [8].

In all the tests, numerical results are in good agreement with the analytical or approximated solutions available, provided that the computational grid approximates the mountain slope sufficiently well. This is shown to be the case for grid spacings that are realistic for high resolution simulations. Furthermore, the efficiency of the proposed method has been demonstrated, since all the main features of dry mountain wave dynamics have been reproduced at reduced computational cost and without any restriction on the steepness of the orography involved.

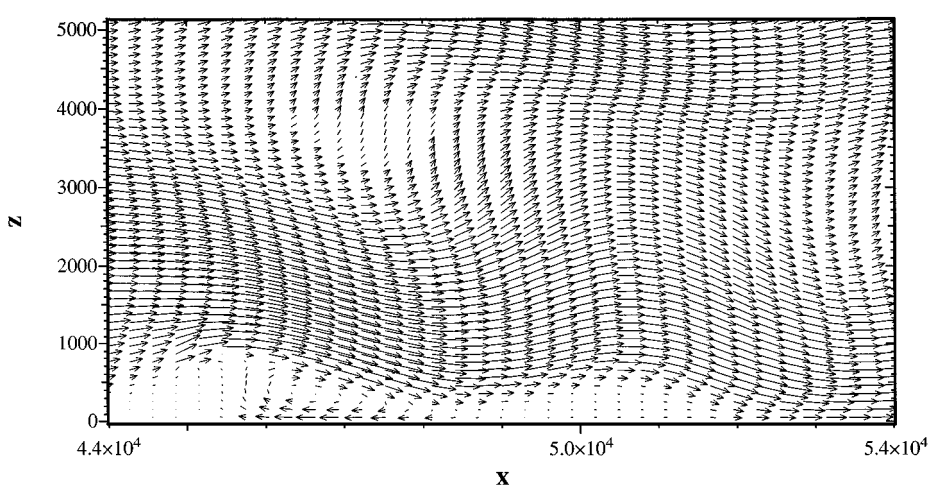

FIG. 20. Velocity field downstream of a thin rectangular obstacle.

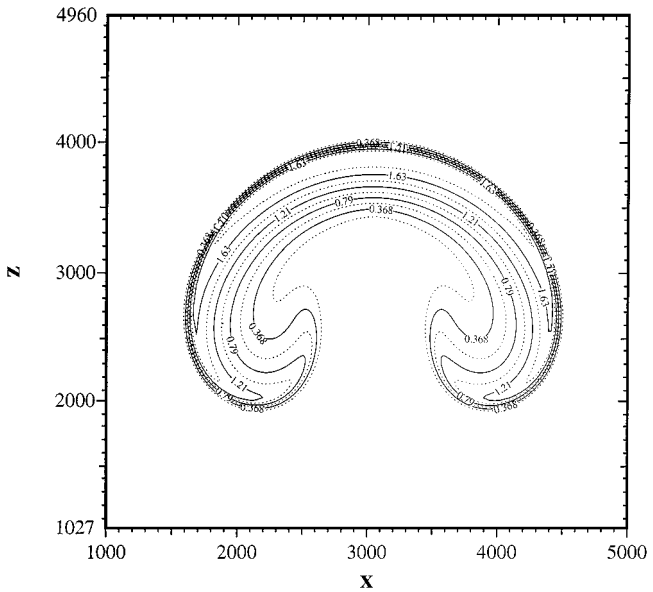

FIG. 21. Potential temperature perturbations in a nonlinear nonhydrostatic time-dependent test case (rising warm bubble in an isentropic atmosphere).

7. CONCLUSIONS

A semi-implicit, semi-lagrangian scheme for the fully elastic, nonhydrostatic equations of atmospheric motion has been developed, using a Cartesian coordinate system with height as the vertical coordinate. No terrain following normalization was employed. As a result, a numerical algorithm is obtained, which only requires the solution of a symmetric and well conditioned system at each timestep. Furthermore, no spurious flows are generated around steep orography. Numerical simulations of well known lee wave test cases demonstrate the efficiency, robustness, and accuracy of the proposed scheme for high resolution mesoscale simulations. Further research work is in progress to perform three-dimensional idealized test cases and to extend the same discretization approach to viscous, moist, and diabatic dynamics.

APPENDIX: WELL POSEDNESS AND STABILITY ANALYSIS

The linearization of Eqs. (6)–(8) around an hydrostatic and stably stratified profile constitutes a well posed initial value problem in the sense of Kreiss (see, e.g., [17, 18]). This well posedness analysis is presented here for completeness, since it has been dealt with in the seminal paper [27] only in the context of the anelastic approximation. The study of the proper initial and boundary value problem is of rather difficult formulation, therefore it will only be shown here that the appropriate frozen coefficient initial value problem is well posed. By the Lax–Richtmyer equivalence theorem, this will then imply convergence of any stable and consistent finite difference approximation of the corresponding linearized equations.

Consider then the linearization of Eqs. (6)–(8) around a constant flow field of components U, V, and 0, respectively, and reference profiles of Exner pressure Π and potential

temperature Θ satisfying $\frac{d\Theta}{dz} > 0$ and the hydrostatic assumption (5). The corresponding constant coefficients linear initial value problem can be obtained by computing Θ, Π, and their derivatives at some fixed value of z. This problem can be written in vector form as

$$\frac{\partial \mathbf{u}}{\partial t} + \mathbf{A}\frac{\partial \mathbf{u}}{\partial x} + \mathbf{B}\frac{\partial \mathbf{u}}{\partial y} + \mathbf{C}\frac{\partial \mathbf{u}}{\partial z} = \mathbf{D}\mathbf{u}, \tag{21}$$

where

$$\mathbf{A} = \begin{bmatrix} U & \frac{\Pi R}{c_v} & 0 & 0 & 0 \\ c_p\Theta & U & 0 & 0 & 0 \\ 0 & 0 & U & 0 & 0 \\ 0 & 0 & 0 & U & 0 \\ 0 & 0 & 0 & 0 & U \end{bmatrix}, \qquad \mathbf{B} = \begin{bmatrix} V & 0 & \frac{\Pi R}{c_v} & 0 & 0 \\ 0 & V & 0 & 0 & 0 \\ c_p\Theta & 0 & V & 0 & 0 \\ 0 & 0 & 0 & V & 0 \\ 0 & 0 & 0 & 0 & V \end{bmatrix}$$

$$\mathbf{C} = \begin{bmatrix} 0 & 0 & 0 & \frac{\Pi R}{c_v} & 0 \\ 0 & 0 & 0 & 0 & 0 \\ 0 & 0 & 0 & 0 & 0 \\ c_p\Theta & 0 & 0 & 0 & 0 \\ 0 & 0 & 0 & 0 & 0 \end{bmatrix}, \qquad \mathbf{D} = \begin{bmatrix} 0 & 0 & 0 & -\frac{d\Pi}{dz} & 0 \\ 0 & 0 & f & 0 & 0 \\ 0 & -f & 0 & 0 & 0 \\ 0 & 0 & 0 & 0 & \frac{g}{\Theta} \\ 0 & 0 & 0 & -\frac{d\Theta}{dz} & 0 \end{bmatrix}, \qquad \mathbf{u} = \begin{bmatrix} \pi \\ u \\ v \\ w \\ \theta \end{bmatrix}.$$

Equation (21) defines a well posed system whose first order part is hyperbolic (see, e.g., [18, 40]). To show this, notice that the symbol of the first order operator applied to $\mathbf{u}$ is given by $\mathbf{Q}(\mathbf{k}) = i\,(k_1\mathbf{A} + k_2\mathbf{B} + k_3\mathbf{C})$, that is,

$$\mathbf{Q}(\mathbf{k}) = i \begin{bmatrix} k_1U + k_2V & \frac{\Pi R k_1}{c_v} & \frac{\Pi R k_2}{c_v} & \frac{\Pi R k_3}{c_v} & 0 \\ c_p\Theta k_1 & k_1U + k_2V & 0 & 0 & 0 \\ c_p\Theta k_2 & 0 & k_1U + k_2V & 0 & 0 \\ c_p\Theta k_3 & 0 & 0 & k_1U + k_2V & 0 \\ 0 & 0 & 0 & 0 & k_1U + k_2V \end{bmatrix}.$$

Introducing the diagonal matrix

$$\mathbf{E} = \begin{bmatrix} \sqrt{c_p\Theta} & 0 & 0 & 0 & 0 \\ 0 & \sqrt{\frac{\Pi R}{c_v}} & 0 & 0 & 0 \\ 0 & 0 & \sqrt{\frac{\Pi R}{c_v}} & 0 & 0 \\ 0 & 0 & 0 & \sqrt{\frac{\Pi R}{c_v}} & 0 \\ 0 & 0 & 0 & 0 & 1 \end{bmatrix},$$

one can notice that $\mathbf{E}\mathbf{Q}\mathbf{E}^{-1}$ is an antisymmetric matrix, whose real coefficients depend linearly on k_1, k_2, k_3. Therefore, $\mathbf{Q}$ has purely imaginary eigenvalues and can be diagonalized uniformly with respect to $|\mathbf{k}|$, so that the conditions for a hyperbolic system are satisfied

and the first order part of the problem is well posed. It is then well known that the addition of lower order terms still keeps the problem well posed; see again [18] for a detailed presentation of these results.

The von Neumann stability analysis of the proposed scheme will now be carried out, showing that linear stability always holds, independently of the timestep chosen. As a consequence of the well posedness of the linearized initial value problem and of the Lax–Richtmyer theorem, the numerical method is then convergent when applied to the constant coefficient linear problem (21). The discretization of Eqs. (21) on a uniform and periodic grid by the method of the previous section yields

$$\begin{aligned}
&\pi^{n+1}_{i,j,k} + \alpha \frac{\Pi R}{c_v} \left(\delta_x u^{n+1} + \delta_y v^{n+1} + \delta_z w^{n+1}\right)_{i,j,k} \Delta t \\
&\quad = (\mathcal{L}\pi)^n_{i,j,k} - (1-\alpha)\frac{\Pi R}{c_v} \mathcal{L}\left(\delta_x u^n + \delta_y v^n + \delta_z w^n\right)_{i,j,k} \Delta t - \mathcal{L}\left(w^n \frac{d\Pi}{dz} \Delta t\right)_{i,j,k} \qquad (22)
\end{aligned}$$

$$u^{n+1}_{i+\frac{1}{2},j,k} + \alpha c_p \Theta \delta_x \pi^{n+1}_{i+\frac{1}{2},j,k} \Delta t = \mathcal{L}(u - (1-\alpha) c_p \Theta \delta_x \pi)^n_{i+\frac{1}{2},j,k} \Delta t \qquad (23)$$

$$v^{n+1}_{i,j+\frac{1}{2},k} + \alpha c_p \Theta \delta_y \pi^{n+1}_{i,j+\frac{1}{2},k} \Delta t = \mathcal{L}(v - (1-\alpha) c_p \Theta \delta_y \pi)^n_{i,j+\frac{1}{2},k} \Delta t \qquad (24)$$

$$\begin{aligned}
&w^{n+1}_{i,j,k+\frac{1}{2}} + \alpha c_p \Theta \delta_z \tilde{\pi}^{n+1}_{i,j,k+\frac{1}{2}} \Delta t - \alpha \frac{g}{\Theta} \Delta t \theta^{n+1}_{i,j,k+\frac{1}{2}} \\
&\qquad = \mathcal{L}\left(w + (1-\alpha)\frac{g}{\Theta}\theta \Delta t - (1-\alpha) c_p \Theta \delta_z \tilde{\pi} \Delta t\right)^n_{i,j,k+\frac{1}{2}} \qquad (25)
\end{aligned}$$

$$\theta^{n+1}_{i,j,k+\frac{1}{2}} + \alpha w^{n+1}_{i,j,k+\frac{1}{2}} \frac{d\Theta}{dz} \Delta t = \mathcal{L}\left(\theta - (1-\alpha) w \frac{d\Theta}{dz} \Delta t\right)^n_{i,j,k+\frac{1}{2}}. \qquad (26)$$

Here, Coriolis terms have been omitted for simplicity. If the discretization of the Coriolis terms is performed by an operator splitting approach, in order to assure the von Neumann stability of the complete scheme it is sufficient to prove it for (22)–(26). Let then the Fourier basis be written as $\exp[I(\omega_1 x + \omega_2 y + \omega_3 z))$ with $I = \sqrt{-1}$ and denote the Fourier coefficients by $\hat{\pi}^n, \hat{u}^n, \hat{v}^n, \hat{w}^n, \hat{\theta}^n$. Applying the above discrete equations to the Fourier series representation of the solution of Eq. (21) yields then

$$\begin{aligned}
&\hat{\pi}^{n+1} + 2\alpha \frac{\Pi R}{c_v} \left[\frac{\hat{u}^{n+1}}{\Delta x} \sin\left(\frac{\omega_1 \Delta x}{2}\right) + \frac{\hat{v}^{n+1}}{\Delta y} \sin\left(\frac{\omega_2 \Delta y}{2}\right) + \frac{\hat{w}^{n+1}}{\Delta z} \sin\left(\frac{\omega_3 \Delta z}{2}\right)\right] I \Delta t \\
&\quad = F\left\{\hat{\pi}^n - 2(1-\alpha) I \left[\frac{\hat{u}^n}{\Delta x} \sin\left(\frac{\omega_1 \Delta x}{2}\right) + \frac{\hat{v}^n}{\Delta y} \sin\left(\frac{\omega_2 \Delta y}{2}\right)\right.\right. \\
&\qquad \left.\left. + \frac{\hat{w}^n}{\Delta z} \sin\left(\frac{\omega_3 \Delta z}{2}\right)\right] \Delta t - \hat{w}^n \frac{d\Pi}{dz} \Delta t\right\} \qquad (27)
\end{aligned}$$

$$\hat{u}^{n+1} + 2\alpha c_p \Theta \frac{\hat{\pi}^{n+1}}{\Delta x} \sin\left(\frac{\omega_1 \Delta x}{2}\right) I \Delta t = F\left[\hat{u}^n - 2(1-\alpha) c_p \Theta \frac{\hat{\pi}^n}{\Delta x} \sin\left(\frac{\omega_1 \Delta x}{2}\right) I \Delta t\right] \qquad (28)$$

$$\hat{v}^{n+1} + 2\alpha c_p \Theta \frac{\hat{\pi}^{n+1}}{\Delta y} \sin\left(\frac{\omega_2 \Delta y}{2}\right) I \Delta t = F\left[\hat{v}^n - 2(1-\alpha) c_p \Theta \frac{\hat{\pi}^n}{\Delta y} \sin\left(\frac{\omega_2 \Delta y}{2}\right) I \Delta t\right] \qquad (29)$$

$$\hat{w}^{n+1} + 2\alpha c_p \Theta \frac{\hat{\pi}^{n+1}}{\Delta z} \sin\left(\frac{\omega_3 \Delta z}{2}\right) I \Delta t - \frac{\alpha g}{\Theta} \hat{\theta}^{n+1} \Delta t$$
$$= F\left[\hat{w}^n - 2(1-\alpha) c_p \Theta \frac{\hat{\pi}^n}{\Delta z} \sin\left(\frac{\omega_3 \Delta z}{2}\right) I \Delta t + \frac{(1-\alpha) g}{\Theta} \hat{\theta}^n \Delta t\right] \tag{30}$$

$$\hat{\theta}^{n+1} + \alpha \frac{d\Theta}{dz} \hat{w}^{n+1} \Delta t = F\left(\hat{\theta}^n - (1-\alpha) \frac{d\Theta}{dz} \hat{w}^n \Delta t\right), \tag{31}$$

where F is now the amplification factor of the interpolation operator at the foot of the characteristics. Equations (27)–(31) can be written in matrix notation as

$$\mathbf{A}\hat{\mathbf{u}}^{n+1} = \mathbf{B}\hat{\mathbf{u}}^n + \mathbf{C}\hat{\mathbf{u}}^n \Delta t,$$

where the matrices **A**, **B**, **C**, **u** are defined as

$$\mathbf{A} = \mathbf{I} + \alpha \Delta t \mathbf{M}, \qquad \mathbf{B} = F(\mathbf{I} - (1-\alpha)\Delta t \mathbf{M})$$

$$\mathbf{C} = \begin{bmatrix} 0 & 0 & 0 & -F\frac{d\Pi}{dz} & 0 \\ 0 & 0 & 0 & 0 & 0 \\ 0 & 0 & 0 & 0 & 0 \\ 0 & 0 & 0 & 0 & 0 \\ 0 & 0 & 0 & 0 & 0 \end{bmatrix}, \qquad \hat{\mathbf{u}}^n = \begin{bmatrix} \hat{\pi}^n \\ \hat{u}^n \\ \hat{v}^n \\ \hat{w}^n \\ \hat{\theta}^n \end{bmatrix},$$

and **M** is given by

$$\begin{bmatrix} 0 & 2\frac{\Pi R}{c_v \Delta x} \sin\left(\frac{\omega_1 \Delta x}{2}\right) I & 2\frac{\Pi R}{c_v \Delta y} \sin\left(\frac{\omega_2 \Delta y}{2}\right) I & 2\frac{\Pi R}{c_v \Delta z} \sin\left(\frac{\omega_3 \Delta z}{2}\right) I & 0 \\ 2\frac{c_p \Theta}{\Delta x} \sin\left(\frac{\omega_1 \Delta x}{2}\right) I & 0 & 0 & 0 & 0 \\ 2\frac{c_p \Theta}{\Delta y} \sin\left(\frac{\omega_2 \Delta y}{2}\right) I & 0 & 0 & 0 & 0 \\ 2\frac{c_p \Theta}{\Delta z} \sin\left(\frac{\omega_3 \Delta z}{2}\right) I & 0 & 0 & 0 & -\frac{g}{\Theta} \\ 0 & 0 & 0 & \frac{d\Theta}{dz} & 0 \end{bmatrix}.$$

The amplification matrix for the scheme in Eqs. (22)–(26) is then given by

$$\mathbf{A}^{-1}\mathbf{B} + \mathbf{A}^{-1}\mathbf{C}\Delta t.$$

Introduce now the diagonal matrix

$$\mathbf{E} = \begin{bmatrix} \sqrt{c_p \Theta} & 0 & 0 & 0 & 0 \\ 0 & \sqrt{\frac{\Pi R}{c_v}} & 0 & 0 & 0 \\ 0 & 0 & \sqrt{\frac{\Pi R}{c_v}} & 0 & 0 \\ 0 & 0 & 0 & \sqrt{\frac{\Pi R}{c_v}} & 0 \\ 0 & 0 & 0 & 0 & I\sqrt{\frac{\Pi R}{c_v} \frac{\Theta}{g} \Big/ \frac{d\Theta}{dz}} \end{bmatrix}$$

and notice that $\mathbf{EME}^{-1}$ is an antisymmetric matrix, which is then diagonalizable and has purely imaginary eigenvalues. Therefore, $\mathbf{M}$ can be diagonalized by some invertible matrix $\mathbf{T}$ and will also have purely imaginary eigenvalues. Furthermore, it is easy to see that also $\mathbf{A}$, $\mathbf{B}$ will be diagonalized by $\mathbf{T}$. Denoting with $I\mu$ the generic eigenvalue of $\mathbf{M}$, where μ is a real number, it follows then that eigenvalues λ of $\mathbf{A}$ must satisfy

$$\lambda = 1 + I\alpha\mu\Delta t,$$

so that $|\lambda| \geq 1$ and $\|\mathbf{A}^{-1}\| \leq 1$ uniformly in ω, where now $\|\cdot\|$ denotes the matrix norm subordinate to the euclidean vector norm, which coincides with the spectral radius for normal matrices, such as $\mathbf{A}$, $\mathbf{B}$, and $\mathbf{A}^{-1}$ are. This implies that

$$\|\mathbf{A}^{-1}\mathbf{C}\| \leq \left|\frac{d\Pi}{dz}\right| \tag{32}$$

uniformly in ω, so that by standard results in the stability theory of finite difference schemes (see, e.g., [40]) a necessary and sufficient condition for stability is given by

$$\|\mathbf{A}^{-1}\mathbf{B}\| \leq 1.$$

This is equivalent to proving that the solutions of

$$\det(\mathbf{B} - \lambda\mathbf{A}) = \det(\mathbf{TBT}^{-1} - \lambda\mathbf{TAT}^{-1}) = 0$$

belong to the unit circle. Since the above equation factorizes, it follows that the eigenvalues λ of $\mathbf{A}^{-1}\mathbf{B}$ must satisfy

$$\lambda = F\frac{1 - (1-\alpha)\mu\Delta t I}{1 + \alpha\mu\Delta t I}.$$

It is then straightforward to prove that for $\alpha \geq \frac{1}{2}$

$$\left|\frac{1 - (1-\alpha)\mu\Delta t I}{1 + \alpha\mu\Delta t I}\right| \leq 1$$

uniformly in ω. Since it can be shown that for all mostly used interpolation schemes the amplification factor $|F| \leq 1$ for all ω (see, e.g., [21]), the desired stability result follows, independently of the order of the interpolation.

ACKNOWLEDGMENTS

This research has been partially supported by the European Commission within the *Training and Mobility of Researchers Program*, Contract ERBFMBICT961555. The author is happy to thank Dr. D. P. Eppel and Professor V. Casulli for their warm encouragement and their great help throughout the work on this project. Many useful discussions on mesoscale models with Dr. H. Kapitza and a great deal of help with *fortran90* data structures and compilers from Dr. A. Rhodin are gratefully acknowledged. The comments of Professor R. Laprise and of two anonymous reviewers were also very helpful in correcting some errors and improving a previous version of this paper.

REFERENCES

1. A. Adcroft, C. Hill, and J. Marshall, Representation of topography by shaved cells in a height coordinate ocean model, *Monthly Weather Rev.* **125**, 2293 (1997).
2. P. Bartello and S. J. Thomas, The cost-effectiveness of semi-Lagrangian advection, *Monthly Weather Rev.* **124**, 2883 (1996).
3. L. Bonaventura, A second order, semi-Lagrangian scheme with accurate approximation of trajectories, in *Proceedings of the 10th International Conference on Numerical Methods for Laminar and Turbulent Flow*, edited by C. Taylor and J. Cross (Pineridge, Swansea, 1997), p. 1.
4. V. Casulli, Semi-implicit finite difference methods for the two-dimensional shallow water equations, *J. Comput. Phys.* **86**, 56 (1990).
5. V. Casulli and E. Cattani, Stability, accuracy and efficiency of a semi-implicit method for three-dimensional shallow water flow, *Comput. Math. Appl.* **27**, 99 (1994).
6. V. Casulli and G. S. Stelling, Numerical simulation of three-dimensional quasi-hydrostatic, free surface flows, *ASCE J. Hydraulic Eng.* **124**(7), 678 (1998).
7. V. Casulli, A semi-implicit finite difference method for nonhydrostatic, free surface flow, *Int. J. Numer. Methods Fluids* **30**(4), 425 (1999).
8. R. L. Carpenter, K. K. Droegemeier, P. R. Woodward, and C. E. Hane, Application of the piecewise parabolic method to meteorological modeling, *Monthly Weather Rev.* **118**, 586 (1990).
9. M. J. P. Cullen, A test of a semi-implicit integration technique for a fully compressible nonhydrostatic model, *Quart. J. R. Met. Soc.* **116**, 1253 (1990).
10. B. W. Golding, An efficient non-hydrostatic model, *Meteorol. Atmosph. Phys.* **50**, 89 (1992).
11. P. Hereil and R. Laprise, Sensitivity of internal gravity waves solution to the time step of a semi-implicit semi-Lagrangian nonhydrostatic model, *Monthly Weather Rev.* **124**, 972 (1996).
12. H. Kapitza and D. P. Eppel, The non-hydrostatic model GESIMA, Part I, *Beitr. Phys. Atmosph.* **65**(2), 129 (1992).
13. H. Kapitza and D. P. Eppel, A 3-D Poisson solver based on conjugate gradients compared to standard iterative methods and its performance on vector computers, *J. Comput. Phys.* **68**, 474 (1987).
14. H. Kapitza, Truncated incomplete factorizations for conjugate-gradient methods in two and three dimensions, *Appl. Math. Comp.* **28**, 73 (1988).
15. J. B. Klemp and D. K. Lilly, Numerical simulation of hydrostatic mountain waves, *J. Atmosph. Sci.* **35**, 78 (1978).
16. J. B. Klemp and R. Wilhelmson, The simulation of three-dimensional convective storm dynamics, *J. Atmosph. Sci.* **35**, 1070 (1978).
17. H. O. Kreiss, Initial boundary value problems for hyperbolic systems, *Comm. Pure Appl. Math.* **22**, 277 (1970).
18. H. O. Kreiss and J. Lorenz, *Initial-Boundary Value Problems and the Navier–Stokes Equations* (Academic Press, San Diego, 1989).
19. R. Laprise and W. R. Peltier, On the structural characteristics of steady state finite amplitude mountain waves over bell-shaped topography, *J. Atmosph. Sci.* **64**, 586 (1989).
20. G. Loria, *Spezielle Algebraische und Traszendente Ebene Kurven* (Teubner, Leipzig, 1910).
21. A. McDonald, Accuracy of multiply upstream, semi-Lagrangian advective schemes, *Monthly Weather Rev.* **112**, 1267 (1984).
22. F. Mesinger, Z. Janic, S. Nickovic, D. Gavrilov, and D. G. Deaven. The step-mountain coordinate: Model description and performance for cases of alpine lee cyclogenesis and for a case of an Appalachian redevelopment, *Monthly Weather Rev.* **116**, 1493 (1988).
23. J. W. Miles, Lee waves in a stratified flow. Part 1. Thin barrier, *J. Fluid Mech.* **32**, 549 (1968).
24. J. W. Miles, Lee waves in a stratified flow. Part 2. Semi-circular obstacle, *J. Fluid Mech.* **33**, 803 (1968).
25. J. W. Miles and H. E. Huppert, Lee waves in a stratified flow. Part 3. Semielliptical obstacles, *J. Fluid Mech.* **35**, 481 (1969).

26. J. W. Miles and H. E. Huppert, Lee waves in a stratified flow. Part 4. Perturbation approximations, *J. Fluid Mech.* **35**, 497 (1969).
27. J. Oliger and A. Sundstrom, Theoretical and practical aspects of some initial boundary value problems in fluid dynamics, *SIAM J. Appl. Math.* **35**, 419 (1978).
28. J. P. Pinty, R. Benoit, E. Richard, and R. Laprise, Simple tests of a semi-implicit semi-Lagrangian model on 2D mountain wave problems, *Monthly Weather Rev.* **123**, 3042 (1995).
29. A. Quarteroni and A. Valli, *Numerical Approximation of Partial Differential Equations* (Springer-Verlag, New York/Berlin, 1994).
30. P. J. Rasch, Towards atmospheres without tops, *Quart. J. R. Met. Soc.* **112**, 1195 (1986).
31. C. Rivest, A. Staniforth, and A. Robert, Spurious resonant response of semi-Lagrangian discretizations to orographic forcing, *Monthly Weather Rev.* **122**, 366 (1994).
32. K. Saito, Semi-implicit fully compressible version of the MRI mesoscale nonhydrostatic model, *Geophys. Mag. Ser. 2* **2**(2), 109 (1997).
33. F. H. M. Semazzi, J. H. Quian, and J. S. Scroggs, A global nonhydrostatic semi-Lagrangian atmospheric model without orography, *Monthly Weather Rev.* **123**, 2534 (1995).
34. W. C. Skamarock and J. B. Klemp, Efficiency and accuracy of the Klemp Wilhelmson time splitting scheme, *Monthly Weather Rev.* **122**, 2623 (1994).
35. W. C. Skamarock, P. K. Smolarkiewicz, and J. B. Klemp, Preconditioned conjugate gradient solvers for Helmoltz equations in nonhydrostatic models, *Monthly Weather Rev.* **125**, 587 (1997).
36. A. Staniforth and J. Coté, Semi-Lagrangian integration schemes for atmospheric models—A review, *Monthly Weather Rev.* **119**, 2206 (1991).
37. A. Staniforth, J. Coté, *et al.*, Developing an integrated atmospheric environment modelling system, in *Numerical Methods for Fluid Dynamics V*, edited by K. W. Morton and M. J. Baines (Clarendon, Oxford, 1995).
38. J. Steppeler and M. Minotte, Communication, 3rd International SRNWP Workshop on Nonhydrostatic Modelling, Offenbach, 1999.
39. J. Stoer and R. Bulirsch, *An Introduction to Numerical Analysis*, 2nd ed. (Springer-Verlag, New York/Berlin, 1980).
40. J. C. Strikwerda, *Finite Difference Schemes and PDE* (Wadsworth-Brooks/Cole, Pacific Grove, 1989).
41. H. Sundqvist, On vertical interpolation and truncation in connexion with use of sigma system models, *Atmosphere* **14**, 37 (1976).
42. M. Tanguay, A. Robert, and R. Laprise, A semi-implicit, semi-Lagrangian fully compressible regional forecast model, *Monthly Weather Rev.* **118**, 1970 (1990).
43. M. C. Tapp and P. W. White, A non-hydrostatic mesoscale model, *Quart. J. R. Met. Soc.* **102**, 277 (1976).
44. C. Temperton and A. Staniforth, An efficient two-time-level semi-Lagrangian semi-implicit integration scheme, *Quart. J. R. Meteor. Soc.* **113**, 1025 (1987).
45. G. Tripoli, Communication, 3rd International SRNWP Workshop on Nonhydrostatic Modelling, Offenbach, 1999.